Sensors & Actuators: A. Physical 345 (2022) 113807

Contents lists available at ScienceDirect

Sensors and Actuators: A. Physical

journal homepage: www.journals.elsevier.com/sensors-and-actuators-a-physical

Techniques to enhance the photoacoustic signal for trace gas sensing: A review

Fupeng Wang [a,b,*,1], Yaopeng Cheng [a,1], Qingsheng Xue [a], Qiang Wang [b], Rui Liang [a], Jinghua Wu [a], Jiachen Sun [c], Cunguang Zhu [d], Qian Li [a]

[a] Faculty of Information Science and Engineering, Ocean University of China, Qingdao, China
[b] State Key Laboratory of Applied Optics, Changchun Institute of Optics, Fine Mechanics and Physics, Chinese Academy of Sciences Changchun, 130033, China
[c] School of Information Science and Engineering and Shandong Provincial Key Laboratory of Laser Technology and Application, Shandong University, Qingdao 266237, China
[d] School of Physics Science and Information Technology, Liaocheng University, Liaocheng 252000, China

ARTICLE INFO

Keywords:
Photoacoustic spectroscopy
Photoacoustic enhancement
EDFA
Resonator
Custom tuning fork
Cantilever
Fiber-optic microphone

ABSTRACT

Photoacoustic spectroscopy (PAS), which relies on the detection of absorption-induced acoustic waves, is widely used for gas sensing. This paper summarizes and discusses most of the recent techniques for photoacoustic enhancement throughout the overall process from laser-molecule interaction to acoustic wave detection. Considering the theoretical principle and system composition of PAS gas sensor, we classify photoacoustic enhancing techniques into three aspects. The first one is to enhance the photoacoustic excitation by building up the laser power in terms of the positive proportional relation between the optical power and photoacoustic signal. The second one is to amplify the acoustic strength with various kinds of resonators after the photoacoustic generation. The third approach to further improve the photoacoustic detection is to develop more efficient acoustic transducers, for example, custom tuning fork, cantilever and fiber-optic microphone. Finally, the advantages and limitations of these different techniques are analyzed.

Note: the criterion to distinguish IC-PAS and EC-PAS is that if the photoacoustic cell locates inside the laser cavity or not.

1. Introduction

Detection of trace gas concentration, typically below 100 parts per million (ppm), is crucial across a broad range of applications in atmospheric chemistry, industrial process control, workplace surveillance, combustion processes, detection of toxic, explosive, flammable gases, as well as medical diagnostics [1].

Spectroscopic gas sensing techniques, such as non-dispersive infrared (NDIR), tunable diode laser absorption spectroscopy (TDLAS), cavity ring down spectroscopy (CRDS), have advanced rapidly in recent years. They are often nonintrusive, require little sample preparation, offer real-time data and permit in situ monitoring or remote detection [2]. With the remarkable development in diode laser source and the wavelength modulation spectroscopy (WMS) technique, TDLAS has been maturely applied for numerous gas analytical purposes due to its high sensitivity and selectivity, fast responsibility. To further improve the detection sensitivity of TDLAS, mid-infrared lasers (MIR) are preferred to target the strong fundamental rotation/vibration absorption lines [3–5], whose strength is usually three orders of magnitude higher than that in the near infrared (NIR) band. In addition to the above-mentioned strategies, PAS was introduced to gas sensing field, which is based on the photoacoustic effect discovered by Alexander Graham Bell in 1880 [6]. In a PAS gas sensor, the light is modulated at the wavelength coinciding with an absorption band of the target gas, the gas molecules are excited by absorbing the optical energy and

Abbreviation: **TDLAS**, tunable diode laser absorption spectroscopy; **NDIR**, non-dispersive infrared spectroscopy; **WMS**, wavelength modulation spectroscopy; **QEPAS**, quartz enhanced photoacoustic spectroscopy; **CEPAS**, cavity-enhanced photoacoustic spectroscopy; **EC-PAS**, extra-cavity enhanced photoacoustic spectroscopy; **IC-PAS**, intra-cavity photoacoustic spectroscopy; **FLI-PAS**, fiber-ring laser intra-cavity photoacoustic spectroscopy; **ASE**, amplified spontaneous emission spectrum; **CRDS**, cavity ring down spectroscopy; **PAS**, photoacoustic spectroscopy; **RAM**, residual amplitude modulation; **MDL**, minimum detection limit; **FBG**, fiber Bragg grating; **PZT**, piezoelectric transducer; **SNR**, signal to noise ratio; **EDFA**, erbium doped fiber amplifier; **EDFL**, erbium doped fiber laser.

* Corresponding author at: College of Information Science and Engineering, Ocean University of China, Qingdao, China.
E-mail address: wfp@ouc.edu.cn (F. Wang).

[1] These authors contributed equally to this work.

https://doi.org/10.1016/j.sna.2022.113807
Received 12 May 2022; Received in revised form 6 July 2022; Accepted 7 August 2022
Available online 9 August 2022
0924-4247/

Nomenclature

f_0	resonant frequency or photoacoustic wave frequency.
Δf	full width at half maximum of the resonance profile in frequency domain.
α	absorption coefficient of sample gas.
l	absorption path length.
c	sound velocity.
ρ	material density.
p	pressure.
ε	dielectric constant of sample gas.
Q	quality factor.
A	geometric area.
C	sample gas concentration.
C_E	capacitance.
P	optical power.
V	resonant volume.
E	Young modulus.

subsequently relax to the ground state either through radiation processes, such as spontaneous or stimulated emission, or by means of non-radiative collisional processes in which the energy is transformed into translational energy. In the case of vibrational excitation, the radiative lifetimes of vibrational levels are longer than the time needed for collisional deactivation. Thus, in practice, non-radiative collisional processes play a dominant role and the absorbed energy is completely released as heat, producing localized transient heating and expansion. A sequence of absorption and release of the accumulated optical energy results in a modulation of molecules' spatial density, giving rise to pressure waves, i.e., sound, with the same frequency of the light modulation [7,8]. Usually, this absorption-induced sound is called photoacoustic signal and detected by a sensitive microphone. A vivid schematic illustrating a series of processes during the generation of the photoacoustic signal is presented in Fig. 1. Considering the principle of photoacoustic effect, modulation-demodulation technique is a common strategy in PAS sensing system, thus the light sources are generally modulated in wavelength or intensity.

The unique detection mechanism of PAS wins itself several competitive advantages over other absorption spectroscopy methods. (i) PAS system does not require an optical detector because an acoustic wave is measured instead of the light power as in other common absorption techniques. It makes PAS more compatible with different laser wavelengths [9,10], where a high-performance photodetector is not always available. (ii) The most attractive characteristic of PAS is that the photoacoustic signal scales with absorbed power, i.e., the constant development of high-power lasers directly increase the photoacoustic excitation. (iii) It is worthwhile to note that PAS is a baseline-free technique where the absorbed energy is measured, rather than the strong transmitted radiation background as in TDLAS, which means the dynamic range of amplifier circuits can be fully exploited. Thus, the influence of shot noise, flicker noise, and unwanted optical fringe interferences can be avoided [11,12]. Therefore, PAS is a widely used method for trace gas detection nowadays due to its promising features discussed above.

The conventional PAS approach to detecting the absorption-induced photoacoustic signal utilizes a gas-filled acoustic resonator equipped with an electret or condenser microphone. Mostly, the light modulation frequency matches up with one of the acoustical eigenfrequencies of the resonant cavity, in which case the system acts as an acoustic amplifier because the energy from modulation cycles can be accumulated in a standing wave. Usually, the amplification gain is relate to the value of the quality factor Q of the acoustic resonator, typically in the range of 10–300 [13], as:

$$Q = \frac{f_0}{\Delta f}\# \tag{1}$$

Photoacoustic signal S measured by the microphone, is given by the following equation [14]:

$$S = k\frac{\alpha lCPQ}{f_0 V}\# \tag{2}$$

where k is a constant describing other system parameters of PAS system. This very equation enlighteningly indicates two main directions to enhance the photoacoustic signal. One is the enhancement of optical power P to boost the photoacoustic excitation, and the other is to increase the Q/f_0 ratio and minimize volume of the acoustic resonator.

As for enhancement of optical excitation, the most straightforward ways are to choose higher power laser sources and increase the laser power with optical fiber amplifier. Another approach is to utilize an external cavity for optical power buildup, namely cavity-enhanced photoacoustic spectroscopy (CEPAS). Though ultra-high excitation realized, it is critical to tightly lock the laser frequency to the longitudinal cavity mode by performing extraordinary careful optical design and sophisticated servo loop. To simplify such gas sensing system, intra-cavity photoacoustic spectroscopy (IC-PAS) is introduced. Given the fact that the optical power within the laser cavity, generally, is greatly higher than the output power, gas cell is planted into the laser cavity for intra-cavity absorption, thus making the best of the laser power. Later, fiber-ring intra-cavity photoacoustic spectroscopy, a modification of IC-PAS, was first proposed by Wang et al. in 2017, with edges of easy optical alignment, all-fiber configuration, low insert loss and multiplexing capability [15]. On the other hand, in order to attain acoustic signal

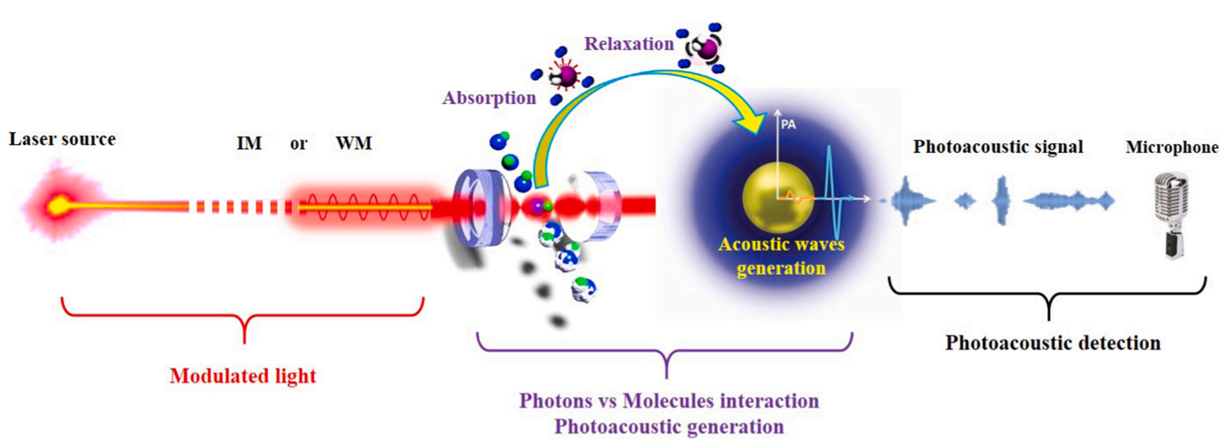

Fig. 1. Schematic of the physical processes occurring within the photoacoustic generation. WM: wavelength modulation, IM: intensity modulation.

amplification and efficient noise suppression, different configurations for acoustic resonators have been developed such as Helmholtz resonators, one-dimensional resonators and differential cavity resonators. Furthermore, QEPAS is an alternative approach to photoacoustic detection of trace gas replacing the microphone with a quartz tuning fork (QTF) to detect weak acoustic excitation. Due to its higher Q/f ratio (two orders of magnitude higher than conventional resonant cavity) and tiny size, QTF is considered as an ideal acoustic resonator for PAS technique at attempt to enhance acoustic signal. The progress in various QEPAS spectrophone configurations further strengthens the acoustic signal. Besides, recently, optics-based acoustic sensing technologies with the merits of high resolution, electromagnetic immunity, large dynamic range and wide frequency band response have been investigated for PAS sensing system. Plus, some special miniaturized cantilevers have been developed to improve the photoacoustic signal detection.

In this review, almost every technique, to our knowledge, proposed to enhance the photoacoustic detection were classified in three aspects. One is the optical power amplification to enhance the photoacoustic excitation which will be introduced in Section 2. The second strategy is acoustic wave enhancement which is summarized in Section 3. In the third aspect, several new-developed acoustic transducers are reviewed in Section 4, such as the custom QTF, cantilever and fiber-optic microphone, to improve the photoacoustic detection sensitivity. In each section, the representative works are discussed and compared to evaluate their advantages and limitations.

2. Strategies to enhance the photoacoustic excitation

2.1. Direct optical power amplification

In terms of the positive proportional relation between the optical power and PA signal as shown in Eq.(2), the sensitivity of PAS systems can benefit from the high output power levels achieved in the development of laser source technology. The implementation of high-power mid-infrared optical frequency comb and QCL lead to considerable improvement in a broadband photoacoustic spectroscopy sensor [16–18]. For example, a blue diode laser with output power level of several watts was reported in 2015 [19]. Two years later, a blue multimode diode laser capable of 3.5 W optical excitation was exploited in a differential photoacoustic cell system by Yin et al. for nitrogen dioxide detection as shown in Fig. 2, of which the (minimum detection limit) MDL of 54 ppt (parts per trillion) was achieved with a 1 s integration time, corresponding to an NNEA of $1.583 \times 10^{-9}\mathrm{cm}^{-1} \bullet \mathrm{W}/\mathrm{Hz}^{1/2}$ owing to the high optical excitation [20].

In addition to selecting high-power light source directly, NIR diode lasers were widely employed in trace gas detection because they are

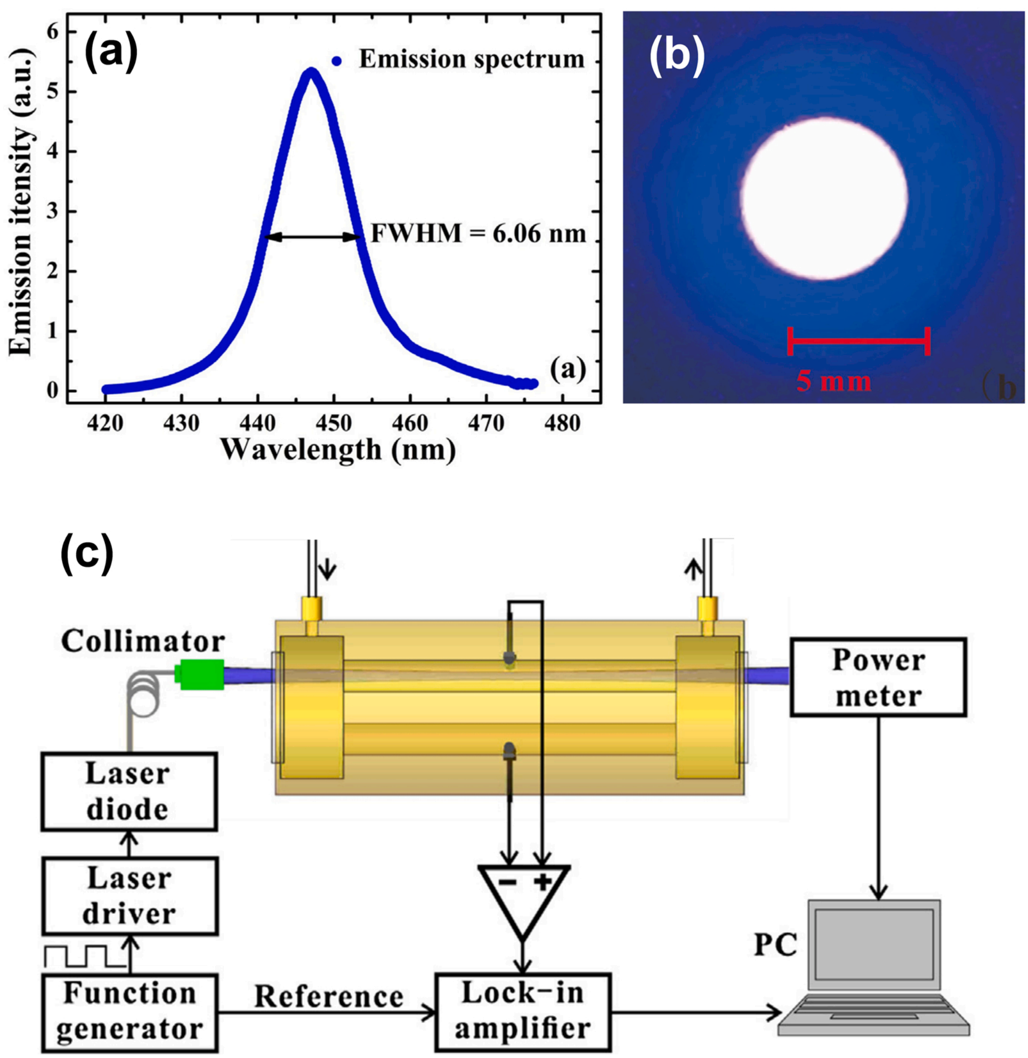

Fig. 2. A 3.5 W blue multimode diode laser used to measure the nitrogen dioxide in a differential photoacoustic cell system. (a) Emission spectrum of the 3.5 W high-power laser diode, (b) Laser beam spot after being shaped by an optical fiber and collimator, (c) The diagram of differential photoacoustic cell NO_2 sensing system. Reprinted from Ref. [20] Copyright (2017) with permission from Elsevier.

inexpensive, long-life (>10 years) and can operate at room temperature. However, the molecular transitions in NIR region are at least 10 times weaker than the fundamental bands in MIR region. Meanwhile, the output power of such NIR diode lasers is on the order of milliwatts. Both factors lead to a weak photoacoustic excitation when using this kind of NIR diode lasers to construct PAS gas sensing system. Fortunately, optical fiber amplification technology widely applied in fiber-optic communication can be used to compensate the sensitivity loss due to the weak absorption line strength in NIR region and the low output power of NIR lasers, for example the erbium doped fiber amplifier (EDFA) technique. The main components of an EDFA are depicted in the middle of Fig. 3, the key component is erbium doped fiber (EDF) fabricated by doping a small amount of erbium into a single mode optical fiber. As a rule, the EDF is pumped with a 980 nm semiconductor diode and up to three orders of amplification factor is easily achieved within the gain bandwidth of the dopant [21]. Afterwards, PAS gas sensing system integrated with an EDFA to boost the laser power before entering the photoacoustic cell, namely fiber-amplifier-enhanced PAS sensors, were demonstrated in many studies [22–28], of which the basic diagram is presented in Fig. 3.

In 2017, Yin et al. introduced the EDFA technique to a differential photoacoustic resonator PAS system for H_2S detection [23]. The probe laser was amplified to 1.36 W successfully, resulting in an MDL of 109 ppb and 281 ppb at 1 s integration time for H_2S gas buffered in SF_6 and N_2 respectively. Similarly, a distributed feedback laser operating at 1532.83 nm was amplified to 1 W, resulting in a detection limit of 0.37 ppb in Prof. Yu's study [24]. The both systems were demonstrated in Fig. 4, EDFA units were inserted between the probe laser seed and photoacoustic excitation location.

In addition to the photoacoustic resonator PAS system, the EDFA method was also applied to QEPAS gas systems [25–28]. In 2015, Wu et al. first proposed a QEPAS-based H_2S gas sensor combining an EDFA with a NIR diode laser [25]. The laser power was boosted to ~1.4 W successfully, furthermore electrical modulation cancellation was performed as shown in Fig. 5(a), ultimately the sensor's MDL was improved to 142 ppb with an integration time of 67 s. In 2017, a long distance, distributed gas sensing using the micro-nano fiber evanescent wave QEPAS technique was reported as shown in Fig. 5(b). To guarantee the long-distance transmission as long as 3 km and the sensor's sensitivity, an EDFA was used to amplified the laser seed to 700 mW. The MDL of three distributed locations were 30 ppm, 51 ppm and 13 ppm respectively along the 3 km detection length. The authors concluded that the sensor's capability can be further improved when an EDFA with a higher output power is available.

In a short summary, benefiting from the increased optical power, the detection sensitivity of PAS sensors can be improved considerably. EDFA is an efficient approach to amplify the laser power. Moreover, there is another advantage to note that the output power of the EDFA is nearly constant within low-frequency wavelength modulation without the residual amplitude modulation (RAM) usually existing in the TDLAS system due to the operating characteristic of semiconductor laser itself.

2.2. Extra-cavity enhanced photoacoustic spectroscopy

To further improve the sensitivity of PAS gas detection, a variety of extra cavities designed for the purpose of multi-pass system and optical power buildup were introduced in photoacoustic resonator PAS system. The multi-pass optical structure can increase the effective interaction path length and the number of passes, meanwhile higher laser power is accumulated during the multi-pass transmission, exciting a stronger photoacoustic signal. In 2005, Song et al. designed a multi-pass optical system, as depicted in Fig. 6(a), of which the number of optical passes were estimated to be eight, leading to a photoacoustic enhancement of 8 folds in water vapor detection. Particularly, the resonator had a differential configuration to reduce the influence of ambient acoustic noise in this study [29,30]. Based on the multi-pass schematic, extra optimization of resonator design was investigated by Hao et al. as shown in Fig. 6 (b). Compared to conventional Herriott configuration, it is more compact and easier to construct and align. A 114-passes arrangement was achieved and the power of the laser in the cell was increased by 45 times [31]. In addition to the spherical mirrors, prism was also used to realize the multi-pass function as reported in Ref. [32] and Ref. [33]. However, the number of passes is limited by the dimension of the prisms.

If a narrow line width laser is coupled into a high finesse optical cavity, a significant power buildup proportional to the finesse value will occur inside the cavity. Based on this very idea, CEPAS technique was introduced and substantially strengthened the photoacoustic signal. In 2005, Rossi et al. performed the pioneering research by combining a Fabry-Perot cavity and a 1 mW diode laser, achieving an effective gain factor of 100 in optical excitation as shown in Fig. 7(a) [34]. Afterwards, a V-shaped cavity with three mirrors was introduced by Kachanov et al. as depicted in Fig. 7(b), in which a MIR external cavity quantum cascade laser (EC-QCL) with an output power of 53 mW was selected as the laser seed. Unlike the linear cavity mentioned above, the direct back-reflections from the cavity to the laser can be avoided. With the assistance of optical feedback locking between the V-shaped cavity and the EC-QCL seed, an optical power buildup factor of 181 was realized [35]. In 2010, Hippler et al. demonstrated a cavity-enhanced PAS system with optical feedback locking technique for ultra-trace gas detection and high-resolution spectroscopy. An optical power about 840 times higher than the laser output was built inside the cavity [2]. Recently, Borri et al. developed a novel bow-tie optical cavity to the QEPAS gas sensing system as shown in Fig. 7(d). A DFB-QCL with an output of 1.5 mW was integrated with the bow-tie optical cavity. As a result, the detection sensitivity was improved by a factor of 500 by virtue of that a high finesse exceeding 1500 was achieved within the bow-tie optical cavity [17,36,37]. In addition to the above studies, some other strategies were developed to lock a high fineness cavity for PAS detection. Especially in a Pound-Drever-Hall locking structure [38], a NNEA of $1.1 \times 10^{-11} cm^{-1} WHz^{-1/2}$ was achieved.

Obviously, since high laser power is always preferred for strong photoacoustic signals, the use of external cavity for multi-pass system or optical buildup was proved to enhance the sensitivity of the PAS sensors

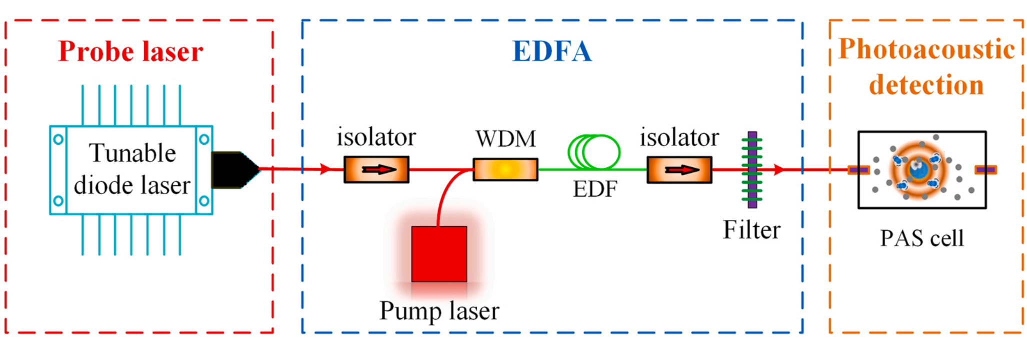

Fig. 3. The basic diagram of EDFA-based photoacoustic detection system.

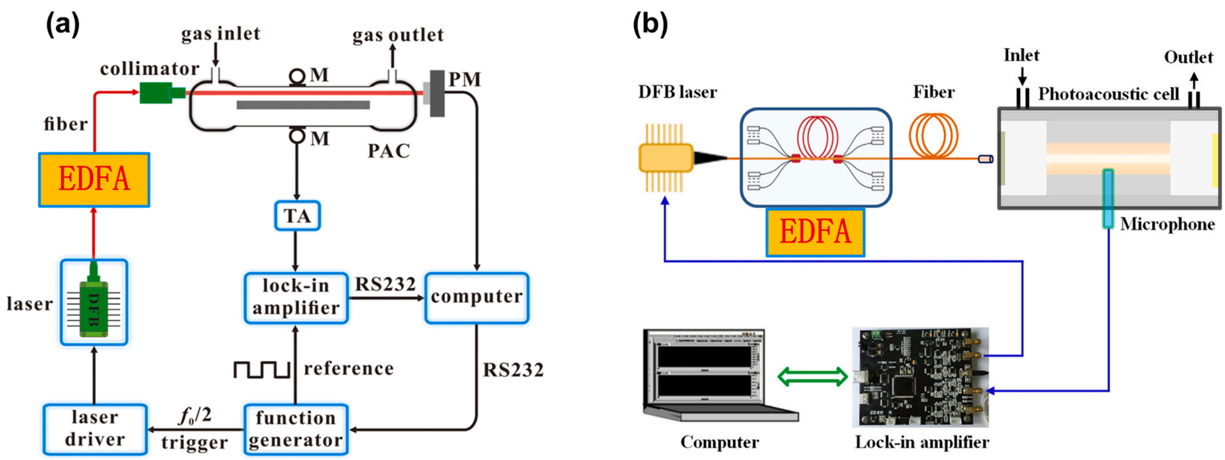

Fig. 4. The diagram of using EDFA in photoacoustic resonator PAS gas sensing system. Reprinted from Ref. [23] with the permission of AIP Publishing. Reprinted from Ref. [24] Copyright (2018) with permission from Elsevier.

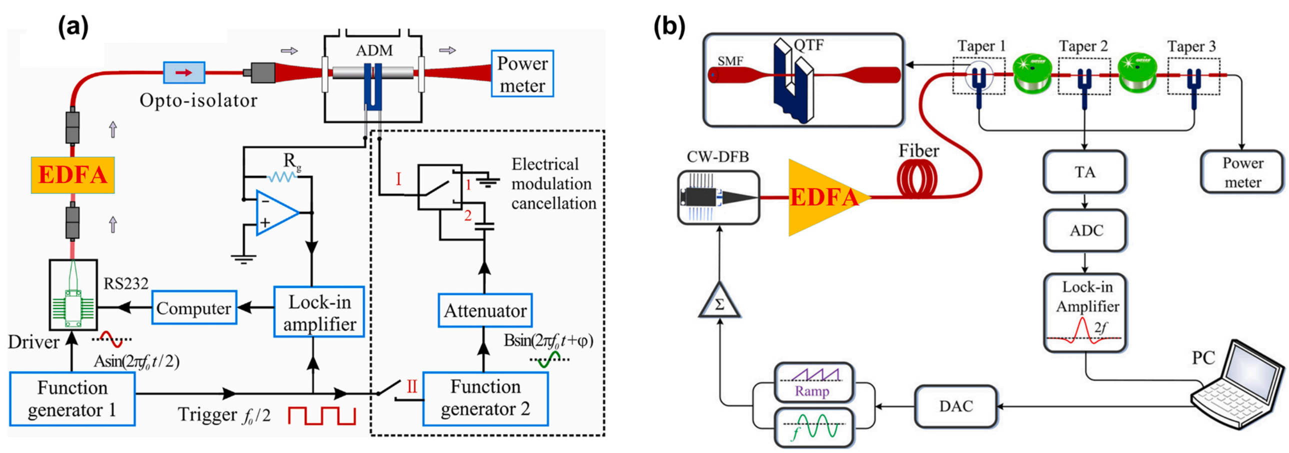

Fig. 5. The EDFA technology used in QEPAS-based gas sensing system. Reprinted from Ref. [25] Copyright (2015) with permission from Elsevier. Reprinted from Ref. [26] with the permission of AIP Publishing.

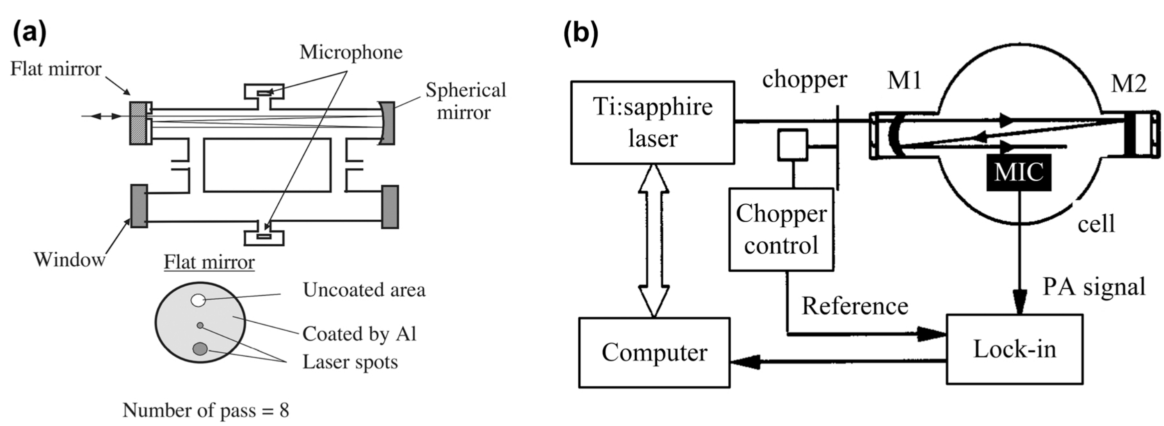

Fig. 6. Schematic of two multi-pass optical systems. (a) A differential multi-pass photoacoustic cell, the number of passes is 8. Reprinted from Ref. [29] Copyright (2005) with permission from Elsevier. (b) An orthogonal cylindrical mirror based multi-pass photoacoustic cell, the number of passes is 114. Reprinted from Ref. [31] with the permission of AIP Publishing.

notably. However, in these extra-cavity enhanced systems discussed above, efficient optical alignment and frequency matching between the laser beam and the optical cavity were necessary. As a result, ultra-precise optical design and sophisticated feedback controller are strictly required in order to actively lock the cavity resonance to the modulated frequency, which is very challenging in practical operation. To simplify such complicated design, techniques merging PAS detection with intra-cavity absorption was reviewed in the next section.

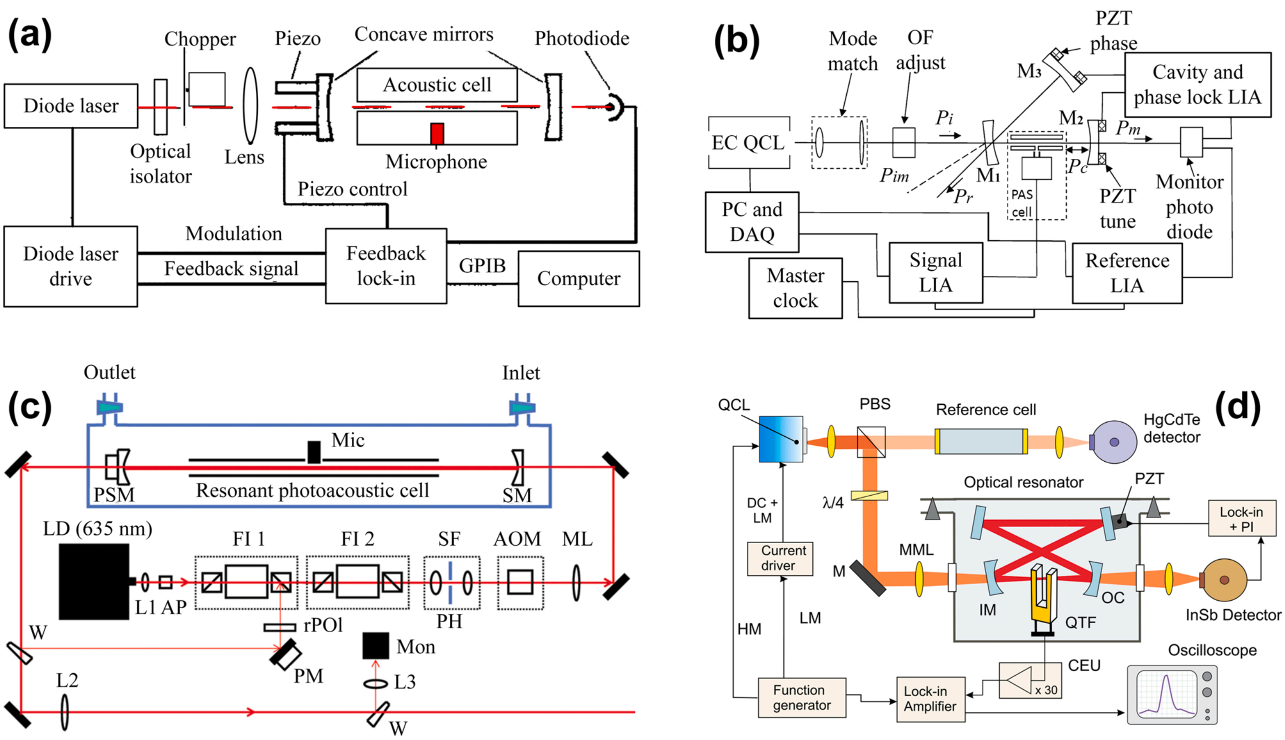

Fig. 7. Schematic of several extra-cavity enhanced optical-feedback-assisted PAS sensors. (a) A Fabry-Perot linear resonator using a PZT-based feedback lock-in controller. Reprinted from Ref. [34] with the permission of AIP Publishing. (b) An optical-feedback V-shaped cavity. Reprinted from Ref. [35] Copyright (2012) with permission from Elsevier. (c) A ring cavity using optical-feedback. Reprinted from Ref. [2] with the permission of AIP Publishing. (d) A feedback-controlled bow-tie optical cavity. Reprinted from Ref. [17] with the permission of AIP Publishing.

2.3. *Intra-cavity enhanced photoacoustic spectroscopy*

Considering that the optical power in the laser cavity, normally, is much higher than the output power. To fully make use of the high power-density within the laser intra-cavity, photoacoustic cells were inserted into the laser intra-cavity to excite a strong acoustic wave. As early as 1987, Röper et al. made the first attempt by placing a cylindrical acoustic resonator in a 3.39 μm He-Ne laser cavity as shown in Fig. 8(a) [39]. A signal enhancement of 2 times was attained in comparison with the conventional extra-cavity operation. However, MIR gas lasers were bulky, expensive and complex apparatuses, which restricted its wide-spread application to such intra-cavity PAS systems. Afterwards, other

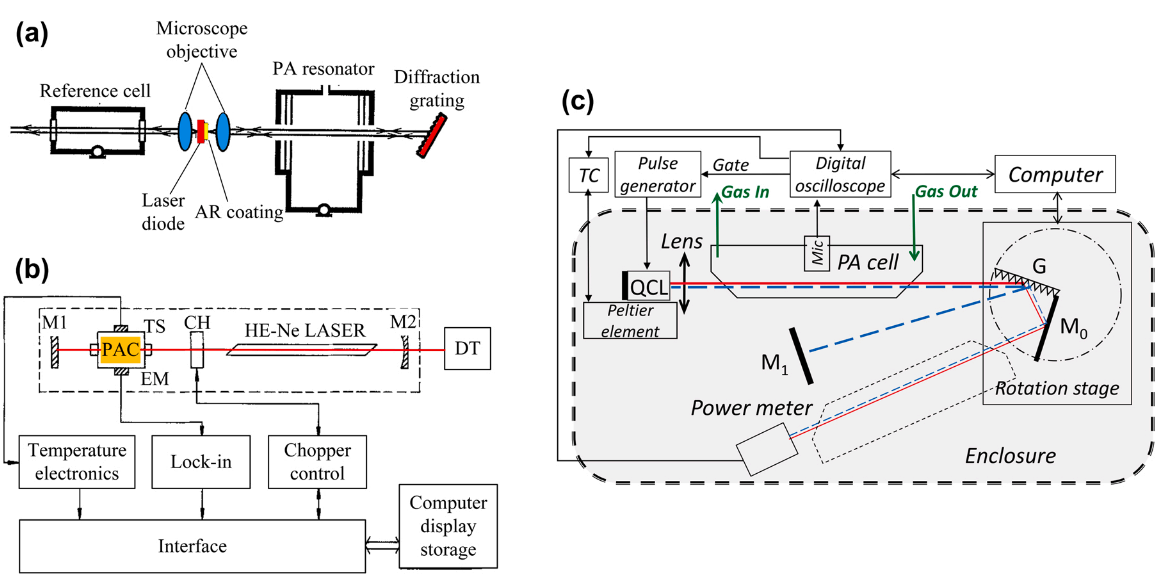

Fig. 8. Schematic of several intra-cavity enhanced PAS sensors. (a) The photoacoustic cell was inserted inside the Fabry-Perot type He-Ne laser cavity. Reprinted from Ref. (b) The photoacoustic resonator was inserted inside the Littrow type external cavity diode laser. Reprinted from Ref. (c) The photoacoustic cell was inserted inside a Littrow type (thick red solid line) or Littman–Metcalf type (thick blue dashed lines) laser cavity. Reprinted from Ref. (For interpretation of the references to colour in this figure legend, the reader is referred to the web version of this article.)

(a) [39] Copyright (1969) with permission from Springer Nature. (b) [40] Copyright (1996) with permission from Springer Nature. (c) [41] Copyright (2016) with permission from Optical Society of America.

types of laser sources were investigated and turned out to be feasible for intra-cavity enhancement. In 1996, Bozóki et al. reported the first use of a NIR diode laser operating at 1.13 μm for intracavity absorption as shown in Fig. 8(b) [40], in which a ten times higher PA signal was observed. Recently, Starovoitov et al. constructed an intra-cavity PAS system utilizing a continuously tunable external cavity QCL operating near 5.5 μm as shown in Fig. 8(c). Two intra-cavity working modes were realized based on the Littrow cavity design and Littman-Metcalf design. As a result, a power enhancement of 80–100 and 140–320 were achieved when the system operating at Littrow mode and Littman-Metcalf mode respectively [41].

2.4. Fiber-ring laser intra-cavity enhanced photoacoustic spectroscopy

Recently, fiber lasers gradually became accessible at a broad wavelength range of NIR region as the rare-earth doped fiber development. Such fiber lasers cover rich absorption features of numerous important gas species such as CO_2, CO, NH_3, H_2S, H_2O and C_2H_2 [42], which provide opportunities to realize gas sensing with compact and flexible configuration. In addition, one of the advantages of fiber lasers is that they are super easy to construct. The photoacoustic resonators or cells can be embedded into fiber lasers cavity conveniently by fiber splicing. In recent years, researchers from Prof. Chang and Prof. Ren's groups proposed several ideas that introducing the photoacoustic cell into the intra-cavity of fiber lasers to make use of the high optical power density, and had published a series of papers on it. In 2017, Wang et al. introduced a fiber-ring laser intra-cavity photoacoustic spectroscopy (FLI--PAS) technique to detect acetylene (C_2H_2) as depicted in Fig. 9(a) [15]. The FLI-PAS sensor mainly consisted of a tunable erbium-doped fiber laser (EDFL) and a transmission-type gas cell. The EDFL was optically pumped by a 980 nm laser diode and its intra-cavity power was built up to 108 mW. A fiber Bragg grating (FBG)-based wavelength modulator was made to perform the WMS by tuning the FBG with a high-speed piezoelectric transducer (PZT) actuator. As a result, the sensor achieved an MDL of 390 ppbv at 2 s integration time for C_2H_2 detection. Afterwards in 2018, Wang et al. introduced the invented FLI-PAS into QEPAS system by utilizing a custom QTF operating at 7.2 kHz as shown in Fig. 9(b), in which the intra-cavity absorption length was reduced to 1.5 cm and significantly extending the linear dynamic range of the gas detection to an order of 10^5. A minimum detectable C_2H_2 concentration of 29 ppbv at 300 s integration time was achieved [43].

Considering the results from Wang's study, higher laser power was accumulated in the intra-cavity of fiber-ring, enhancing the photoacoustic strength dramatically. However, the laser power was continuous output. Therefore, the laser power outside the absorption bandwidth of target gas did not contribute to the excitation of photoacoustic signal. As a result, a large part of laser energy was of no avail. As we know, the laser Q-switching technology is regarded as an effective approach to obtain a high-power output [44–46]. In order to make full use of the pump power and the intra-cavity laser energy, the operating wavelength of fiber-ring laser was locked at the center of target absorption profile, simultaneously the Q-switching technique was applied to the fiber-ring laser intra-cavity enhanced QEPAS system by Zhang et al. in 2019 [47]. The wavelength locking was realized by a temperature-controlled FBG as shown in Fig. 10 (a), a fast acoustic-optical modulation (AOM) was employed in the laser cavity as the Q-switch. The system achieved a maximum peak pulse in excess of 6 W and an MDL of 101 pptv at 20 ms integration time for C_2H_2 detection. To acquire the complete absorption curve instead of only measuring the maximum value at the absorption center as reported in reference [47], a DFB laser seed operating at 1532.83 nm was coupled into the fiber-ring laser cavity to realize the wavelength scanning [48]. It should be noted that a $\Delta\lambda \approx 500pm$ FBG centered at 1532.83 nm was stilled needed to pre-defined the wavelength bandwidth as shown in Fig. 10 (b), so that the laser seed can win the competitive advantage among the pumped spontaneous emission. As a result, a peak power of 0.88 W was observed and an MDL was derived to be 32 ppbv at an integration time of 268 s for C_2H_2 gas.

Even the wavelength scanning technique and active Q-switching technology have been combined together in QEPAS system to measure the C_2H_2 concentration as mentioned in Zhang's study [48], and the wavelength scanning is very easily realized by an external seed laser. However, additional FBG is still needed to stabilize the intra-cavity operation and suppress the amplified spontaneous emission (ASE) spectrum. As a result, the system is very complex and lots of insertion losses are introduced to the laser cavity as depicted in Fig. 10 (b), so the peak power of only 0.88 W was obtained under the same pump power compared with Fig. 10 (a). Very recently, we presented a new fiber-ring laser intra-cavity enhanced QEPAS system with a more efficient approach to realizing the wavelength scanning as shown in Fig. 11 (a). In this study, a custom FBG is attached to a PZT to realize the wavelength selection and scanning. The procedure of fabricating the FBG-based PZT module was demonstrated in detail as depicted in Fig. 11 (b), and we believe this would be instructive for researchers to perform the similar study. In addition, the wavelength and power response characteristics of the fiber-ring laser and its influence on the photoacoustic detection were studied in detail for the first time. A very important conclusion is drawn that the intra-cavity peak power is the decisive factor to excite a stronger photoacoustic signal rather than the average power which can be proved by the data in Fig. 11 of the paper [49]. As a result, up to ~3 W

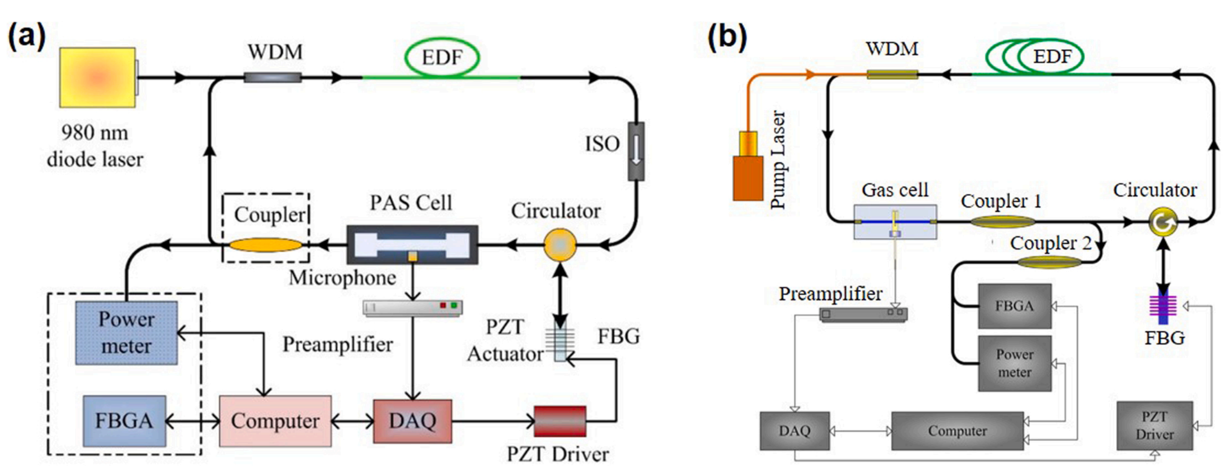

Fig. 9. Two schematics of fiber-ring laser intra-cavity enhanced photoacoustic spectroscopy used in conventional photoacoustic resonator PAS system (a) and QEPAS system (b), the wavelength modulation spectroscopy technique was performed by a PZT module. Reprinted from Ref.
(a) [15] Copyright (2017) with permission from Optical Society of America, and Ref. (b) [43] Copyright (2018) with permission from Elsevier.

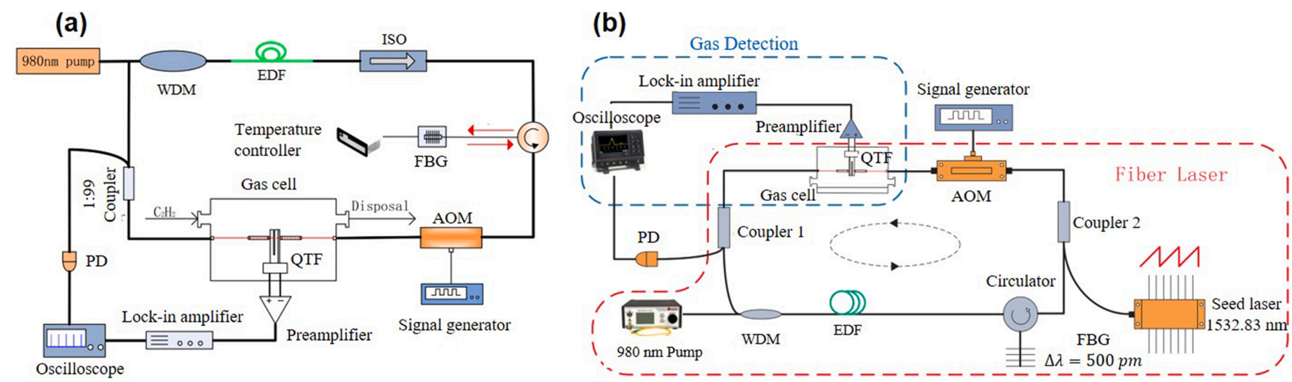

Fig. 10. Two schematics of fiber-ring laser intra-cavity enhanced QEPAS system working in the Q-switching mode. (a) The constant wavelength working with Q-switching pulsed output. [47] Copyright (2019) IEEE. (b) Laser-seed-based wavelength scanning working with Q-switching technology. Reprinted from Ref. (a) Reprinted with permission from Ref. (b) [48] Copyright (2019) with permission from Elsevier.

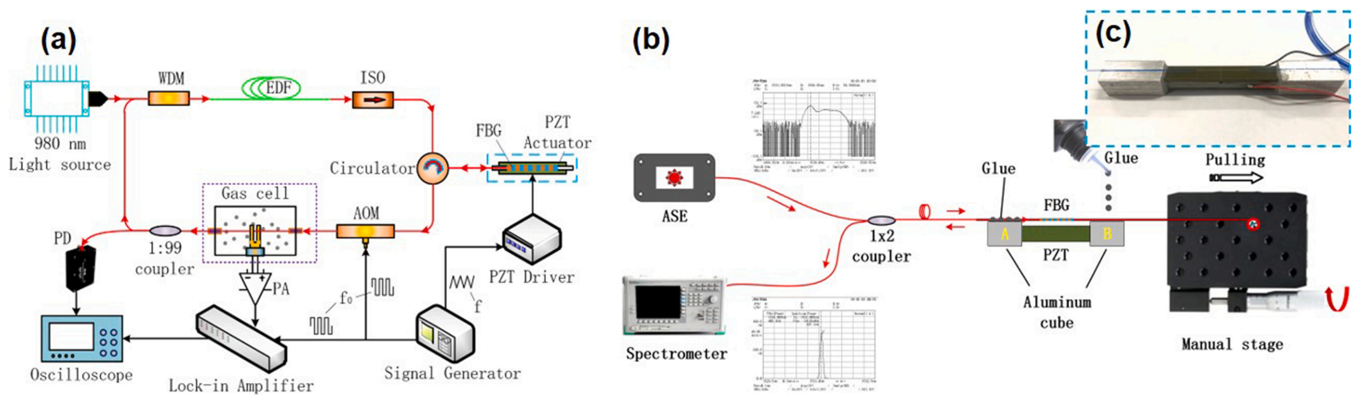

Fig. 11. (a) Configuration of a wavelength scanning Q-switched fiber-ring laser intra-cavity enhanced QEPAS system, (b) The procedure of fabricating the FBG-based wavelength scanning PZT module, (c) The physical picture of the FBG-based wavelength scanning PZT module. Reprinted from Ref. [49] Copyright (2021) with permission from Elsevier.

intra-cavity peak power was achieved with 650 mW pump. In acetylene detection, a noise equivalent concentration of 26 ppbv at 50 ms integration time was achieved.

Summarily, benefiting from the high peak power of Q-switched laser pulse, the photoacoustic signal is substantially enhanced. Moreover, FLI-PAS technique has numerous positive features such as easier optical alignment, all-fiber configuration, multiplexing capability and lower insertion loss. In addition, the FLI-PAS technique could readily extend to MIR region attributed to the advent of the MIR fiber lasers with novel fiber materials (e.g., fluorides, silicates, and chalcogenides) doped with rare-earth ions [50] and the gas-filled silica hollow-core fiber [51].

3. Structures to amplify the acoustic strength

3.1. Resonant photoacoustic cells to amplify the acoustic strength

Section 2 thoroughly reviews the widely used techniques for the enhancement of optical excitation in a bid to improve the photoacoustic effect. In this section, within the detection of photoacoustic signal, a variety of approaches are adopted in PAS sensing systems to enhance the acoustic strength in advance.

In practical applications, photoacoustic measurement is performed in a gas-filled enclosure called "PA cell". If some additional acoustic amplification designs are carried out inside the cell, the boundaries of acoustic resonators give rise to constructive interference, substantially increasing the acoustic wave strength. Usually, PA cell with a high Q/f_0 ratio and small volume is favorable to acquiring stronger acoustic signal according to the Eq.(2). Therefore, based on this very idea, many typical resonant PA cells have been developed as displayed in Fig. 12.

One-dimensional resonant PA cell is the simplest type as shown in Fig. 12 (a), which is applied in the situation where the cross-sectional dimensions are much shorter than the acoustic wavelength that the spatial distribution of the excited sound field is only determined by the length of the one-dimensional tube. The sound wave propagating in the tube is reflected by a closed or open end with the opposite or same phase. If the tube length is equivalent to an integer multiple of the half wavelength, in an open-open ends tube or closed-closed ends tube, resonance will take place and a standing wave will be generated by multiple reflections. However, in practice, the resonance wavelengths are slightly larger. The exact resonant frequencies should be calibrated as [13],

$$f_0 = \frac{qc}{2(L+\Delta L)}, \quad \textit{open} - \textit{open or closed} - \textit{closed ends tube};$$

$$f_0 = \frac{(2q-1)c}{4(L+\Delta L)}, \text{open} - \textit{closedendstube}; \tag{3}$$

$$q = 1, \quad 2, \quad 3, \quad \cdots.$$

The end correction ΔL is a compensation for the mismatch between the one-dimensional acoustic field in the tube and the outside three-dimensional field radiated through the open end. So, for each open end, the end correction ought to be added on the tube length, while the end correction for a closed end is obviously zero. If the tube end opens to a large diameter volume, for example a buffer chamber as shown in Fig. 12 (b), it can be regarded as an ideal open end in terms of its behavior.

Helmholtz PA cell comprises two cavities and an adjoining neck as

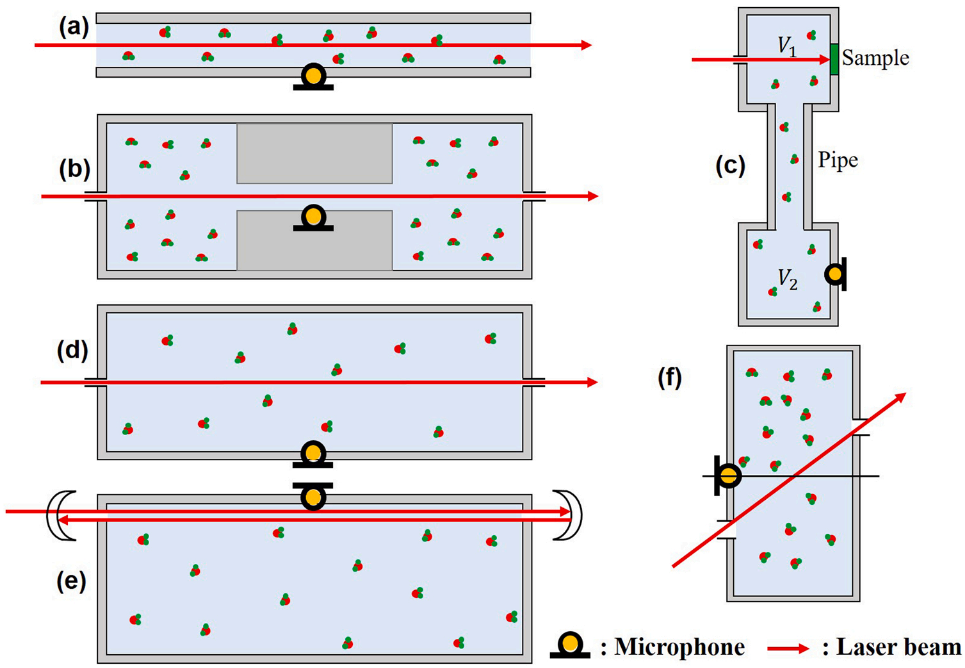

Fig. 12. A series of fundamental resonant PA cells. (a) One-dimensional tube, (b) tube with buffers, (c) Helmholtz PA cell, (d-f) three cylindrical PA cells. Reprinted from Ref. [13] with permission from AIP Publishing.

depicted in Fig. 12 (c). The acoustic equivalent is a simple vibrating system consisting of a mass attached to a spring. The air in the two cavities corresponds to the spring, while the air in the neck acts as the moving mass. When acoustic wave being generated in cavity V_1, the air in the neck moves back and forth with the compression and rarefaction, resulting in a linear elastic restoring force, which helps to return the equilibrium state. This motion gives a single resonant frequency as [52, 53],

$$f_0 = \frac{c}{2\pi}\sqrt{\frac{A}{V_{eff} \times L}}, \quad V_{eff} = \frac{1}{1/V_1 + 1/V_2} \# \tag{4}$$

Where A and L are the neck cross-sectional area and the neck length, respectively. In practical applications, limited by the thermal loss, neck wall loss and radiation loss through the opening for microphone and gas transport, the feasible resonant amplification factor is generally below 10. Moreover, the photoacoustic signal cannot be separated from the background signal originating from nonselective absorption of optical windows. As a result, the sensitivity of Helmholtz PA cells is relatively low.

If cavity dimensions of resonant PA cells are comparable to the acoustic wavelength, several distinct acoustic modes with different standing wave patterns and resonant frequencies can be formed. As a general rule, cavities are designed in certain regular shapes, such as cubes, spheres and cylinders. Among them, the most commonly used cavity is shaped into cylinder as shown in Fig. 12 (d)-(f), because its unique symmetry properly coincides with the laser beam along the cylinder axis, bringing about smaller energy losses. The analytical expression of the resonant frequencies of cylindrical cavity are as follows [54],

$$f_0 = \frac{c}{2}\left[\left(\frac{\alpha_{nm}}{R}\right)^2 + \left(\frac{q}{L}\right)^2\right]^{\frac{1}{2}} \# \tag{5}$$

Where R and L denote the radius and length of the cylinder, α_{nm} is the n_{th} of the derivative at zero of the m_{th} Bessel function divided by π, and the nonnegative integers n, m, q correspond to the eigenvalues of the radial, azimuthal, and longitudinal modes respectively. The acoustic energy in the cavity will gain remarkably as long as it operates at resonant frequencies of these eigenmodes.

Most recently, Gong et al. reported a novel T-shaped acoustic resonator incorporating a cantilever-based fiber-optic microphone, the schematic of which is shown in Fig. 13 [56,57]. The first-order longitudinal resonant frequency of the T-type resonator is defined as,

$$f_0 = \frac{c}{4\left(L + \frac{8}{3\pi}R\right)} \# \tag{6}$$

Where R and L are the radius and length of the resonator. So, the first-order resonant frequency was relatively low, equal to 1368 Hz. Through simulation, the antinode of the acoustic signal was found in tail-end of the resonator just where the fiber-optic microphone was placed. The WMS technique was performed to obtain a higher SNR by suppressing the $1/f$ noise. Furthermore, the acoustic signal was investigated as the function of cell pressure to attain the maximum acoustic strength. As a result, the MDL of the PAS sensor is 156.7 ppb for CH_4 detection at the integration time of 10 s

3.2. Acoustic resonant configurations used in QEPAS system

QEPAS, first demonstrated in 2002 by Kosterev et al. [58], is an alternative method to detect weak photoacoustic signal. Usually, QEPAS comprises commercially available piezoelectric QTF as transducers converting acoustic wave to electric signal efficiently. A laser beams is focused to propagate between the QTF prongs and modulated at the resonant frequency of the QTF. Then, the acoustic wave induced by the photoacoustic effect causes mechanical deformation of the QTF prongs thus producing electrical charges on their electrodes. A trans-impedance amplifier is employed to acquire the QTF electrical response by converting piezoelectric current into voltage. In contrast to the standard PAS approach, acoustic energy accumulates in sharply resonant QTF rather than PA cells. Since the ambient noise shows a $1/f$ dependence, traditional microphone-based PA cells are susceptible to environmental noise for their low resonant frequency (typically < 4 kHz), while QEPAS has excellent background noise immunity attributed to the high resonant frequency and narrow resonance bandwidth of the QTF [14,49].

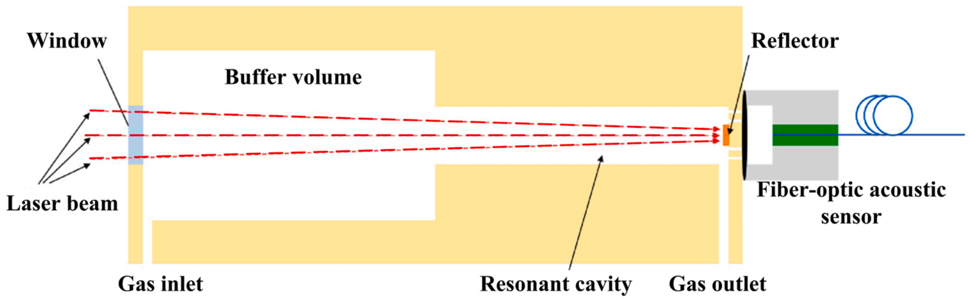

Fig. 13. Schematic of a T-shaped acoustic resonator with particular cantilever-based fiber-optic acoustic sensing. Reprinted from Open Access Ref. [57] which permits unrestricted use, distribution, and reproduction in any medium, provided the original work is properly cited.

Benefited from the high Q factor (70,000–110,000 in vacuum, 10, 000–13,000 in air at normal pressure and room temperature) of the QTF, QEPAS sensors tend to achieve a high SNR. Moreover, the QTF has a tiny size, leading to the reduction of the gas consumption. As a result, QEPAS provides numerous advantages such as ultrahigh sensitivity, fast responsibility, excellent environmental noise immunity and compact integration [59]. In addition to the standard 32.768 kHz QTF, custom-made QTF was investigated for QEPAS detection [60]. Compared to the standard QTF, custom QTF has larger prong spacing (up to 2 mm [61]) and lower resonant frequency (down to 2.8 kHz). The dimensional properties benefit the use of poor-beam-quality laser sources such as mid-infrared lasers, so that the laser beam can pass through without hitting the prongs since otherwise an undesirable noise would arise due to the photothermal effect.

To enhance the photoacoustic signal, micro-resonators (AR) are usually mounted together with the QTF to amplify the acoustic wave strength. The employment of the AR increases the effective interaction length between the radiation-excited acoustic wave and the QTF, thus enhancing the PA signal no matter in standard QTF based or custom QTF based QEPAS system. The QTF together with AR is called the QEPAS spectrophone. Two types of spectrophone configurations have found widespread use in QEPAS sensors so far: on-beam configuration and off-beam configuration. The Fig. 14 displays three kinds of on-beam configurations called dual-tubes on beam, half-tube on beam and single-tube on beam [62–69]. The dual-tubes on-beam configuration as shown in Fig. 14 (a), composed of two metallic thin tubes set perpendicular to the QTF plane, has been developed to be the most frequently used spectrophone in QEPAS sensing system. After a series of optimization, the dual-tubes on-beam configuration can achieve a sensitivity gain factor of ~30 compared with the bare QTF [64,65]. However, the resonant condition for an acoustic wave could not be exactly realized due to the inevitable sound energy loss from the gap between the dual tubes. Additionally, the gap of QTF prongs and inner diameter of resonators constrained the size of the laser beam so that only light sources with high spatial radiation quality are fit for this kind of spectrophone. Then, the careful assembly and optical alignment are still required. To reduce the aforementioned limitations, a simplified version of on-beam configuration named half-tube on-beam as shown in Fig. 14 (b) was reported by Yi et al. and Wang et al. [62,63], similar to the dual-tubes on-beam configuration but easier for assembly and optical alignment. After optimization, it can realize a photoacoustic enhancement factor of ~21 compared to the bare QTF. In 2016, the custom QTF was studied

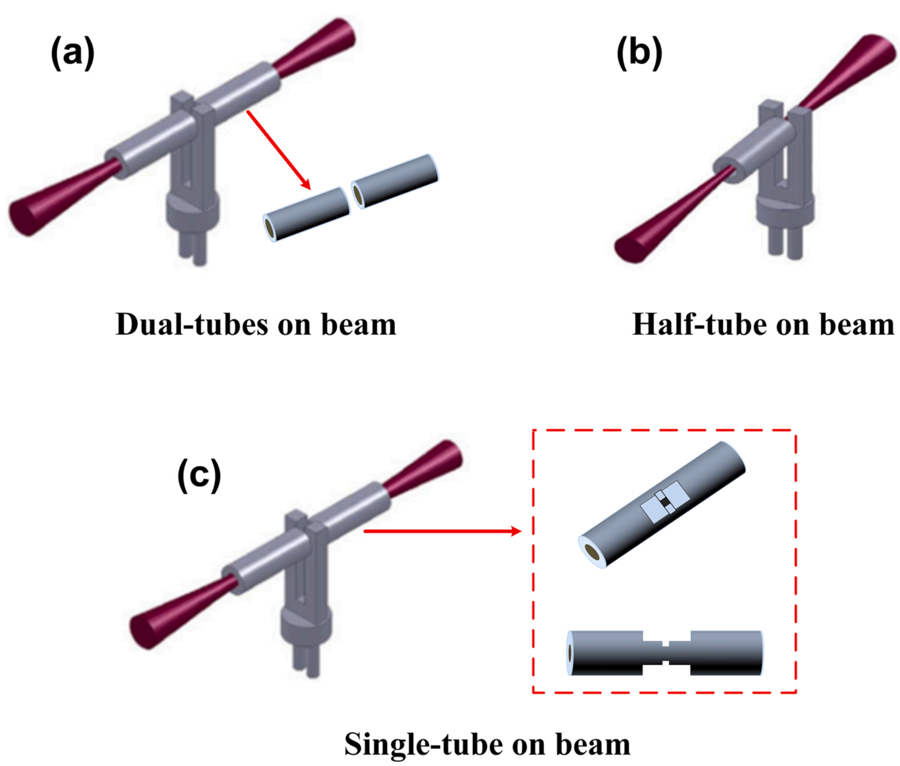

Fig. 14. Commonly used QEPAS acoustic resonant on-beam configurations. (a) dual-tubes on-beam, (b) half-tube on-beam, (c) single-tube on-beam [62–69].

and developed, permitting more spectrophone configurations applied to QEPAS system due to its larger prong spacing (0.4–2 mm) than standard QTF (0.2–0.3 mm). The large dimension of custom QTF gives the way to a novel single-tube on-beam spectrophone as depicted in Fig. 14 (c) to further improve the photoacoustic detection. A pair of slits was symmetrically opened on each side of the tube waist, letting acoustic wave exit from two slits to impact on the internal surface of two QTF prongs. This approach achieved high acoustic coupling efficiency between AR and QTF, as a result, it improved the detection sensitivity by 2 orders of magnitude compared to a bare QTF [66–69].

Configurations reported in Fig. 14 utilized a single light beam to excite the PA signal, afterwards, multi-beams strategy was developed as shown in Fig. 15 to enhance the photoacoustic detection. If the laser 1 and laser 2 as depicted in Fig. 15 (a) worked in different wavelengths, the double laser beams with the adjacent ARs can provide two independent detection channels for different gases [70]. If the laser 1 and laser 2 worked in the same wavelength, a nearly 2-times enhancement was expected by the double laser beams when the synchronism was ensured. Similarly, a right-angle prism can be used to realize the double laser beams as shown in Fig. 15 (b) [71], in the experiment, the four-tubes double-beams configuration enhanced the PA signal by a factor of 22.4 compared with a bare QTF. Most recently, in 2021, a multiple-sound-source-excitation QEPAS based on a single-line spot pattern multi-pass configuration was invented for trace gas detection [72]. This special spectrophone as shown in Fig. 15 (c) produced 60 sound sources between the QTF prongs by making a laser beam pass through the QTF 60 times. As a result, a photoacoustic gain factor of ~20 was achieved. This idea is similar to the multi-pass photoacoustic cell used in the extra-cavity enhanced method as mentioned in Section 2.2.

The on-beam configurations require a very high laser beam quality as discussed in the above paragraph. Another method to circumvent this restriction is using off-beam configurations [73], which allows for larger excitation laser beams and facilitates the optical alignment. In off-beam configurations, the excitation laser beam is coupled through the AR while the QTF is placed external to the AR, close to the slit or branch tube, to probe the photoacoustic signal. The conventional off-beam QEPAS spectrophone was first proposed by Liu et al. in 2009, and three different layouts as displayed in Fig. 16 (a-1, a-2, a-3) were introduced in the paper [74]. The configuration of Fig. 16 (a-1) was chosen to construct a QEPAS-based water vapor detection system and the dimensional parameters of the AR tube were optimized to an optimal

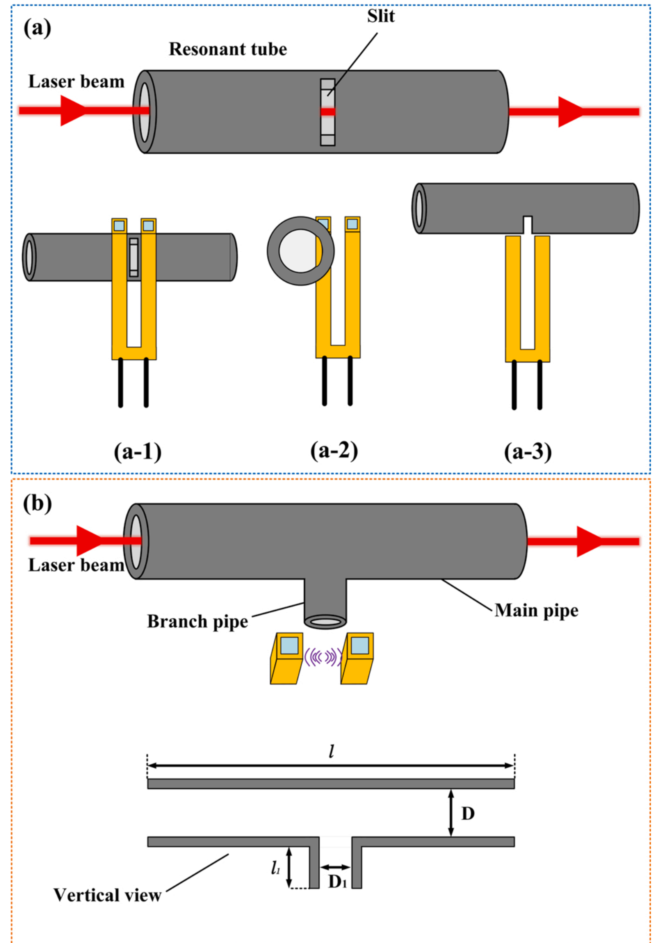

Fig. 16. Two frequently-used off-beam configurations. (a) Diagram of the first off-beam configuration and three placements of QTF a-1, a-2 and a-3. (b) T-shape resonator based off-beam configuration and its critical geometric parameters.

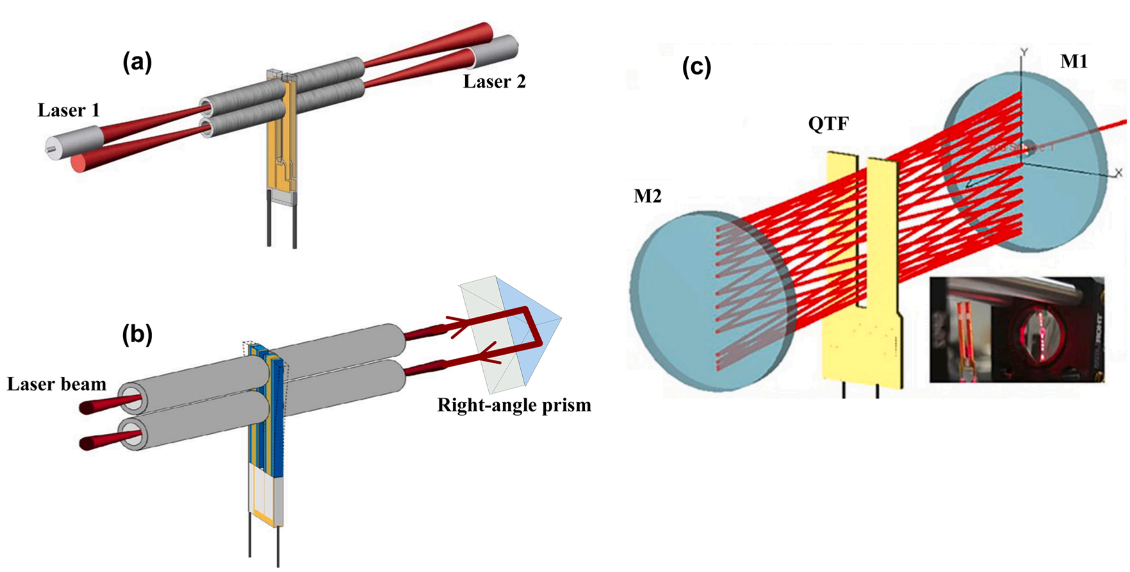

Fig. 15. Multi-beams QEPAS spectrophone configurations. (a) dual-tubes for two independent detection channels, (b) dual-tubes for one detection channel to enhance the acoustic strength, (c) multi-beams configuration to enhance the photoacoustic detection. Reprinted from Ref. [72] with permission from AIP Publishing.

condition, as a result, a photoacoustic signal of ~15.7 times enhancement was achieved compared to a bare QTF in on-beam configuration. Theoretical analysis of off-beam model was also performed by Yi et al. to obtain a formula for numerically calculating the optimal AR parameters, and the calculated results can closely match experimental data [75]. In addition, other researchers also paid a lot of efforts on applying and optimizing the off-beam spectrophone in Fig. 16 (a-1) for NO_2 and C_2H_4 detection [76,77]. In order to achieve a high acoustic coupling efficiency, another off-beam configuration as shown in Fig. 16 (a-2) was proposed, and further developed by Hu et al. as depicted in Fig. 17 (a) [78], the QTF prongs were inserted to the slit of resonant tube to improve the acoustic coupling efficiency, by virtue of a right-angle prism as depicted in Fig. 17 (a), a two-fold photoacoustic enhancement were attained. Recently in 2022, a new in-plane QEPAS sensor with a line interaction mode was reported, which can be classified as a supplement of the off-beam configurations [79]. In this study, a long slit was slotted axially on the sidewall of resonator, the interaction area for the acoustic wave was not limited to a point of the QTF prongs but extended along the whole plane of QTF prongs. As a result, the extended interaction area achieved 4.11 times photoacoustic enhancement.

In addition to the conventional off-beam configuration, a T-shape resonator like Fig. 16 (b) was introduced to the off-beam QEPAS system for the first time in 2012 [80]. Its particular characteristic is that the T-shape resonator consists of an additional short branch pipe in the middle of the long main pipe. The acoustic energy escaped from the short branch pipe is used to push the QTF prongs. After optimization of the parameters such as l, l_1, D, D_1 marked in Fig. 16 (b), the T-shape resonator can increase the photoacoustic signal by a factor of ~30 compared with using only a bare QTF. The result is equal to the performance of frequently-used dual-tubes on-beam structure, however, the T-shape resonator keeps the advantages of off-beam configuration that it is no longer necessary to couple excitation light beam through the narrow QTF prongs. It is easier for optical alignment and spectrophone assembly. Afterwards, a T-shape resonator-based QEPAS system was developed for ambient methane monitoring in 2013. A 1σ detection limit of 400 ppb at an integration time of 10 s was achieved under atmospheric pressure [81]. Very recently, an H-shape AR-based QEPAS spectrophone was first demonstrated as shown in Fig. 17 (b) [82]. The H-shape structure is composed of two T-shape resonators which are placed at either side of the QTF. A dual-beam optical path is realized by utilizing a right-angle prism, which is similar to the studies Fig. 17 (a) published in references [71] and [78]. Compared with a bare QTF system, the H-shape AR-based spectrophone achieved a 17.2 times enhancement. Based on the experience as reported in reference [80], the performance of the H-shape spectrophone could be further improved after parameters optimization.

Conducting a short summary, every acoustic resonant configuration utilized in QEPAS system is based on one or more AR tubes, whether it belongs to on-beam or off-beam structure. Many studies were also performed to evaluate and optimize the geometric parameters of such AR-tube-based spectrophones. Usually, the tube length and inner diameter are the most important parameters determining the photoacoustic enhancement. Because this kind of configuration makes use of the longitude resonance inside the AR tubes for the tube length is usually far longer than its diameter. Hence, careful optical alignment is still necessary no matter in on-beam systems or off-beam ones. Until recently in 2021, Lv et al. proposed a radical-cavity QEPAS sensor in which researchers designed a radial-cavity to enhance the acoustic strength. The radial-cavity is manufactured with aluminum material, characterized with an optimum length of 6.9 mm and a radius of 6.4 mm [83]. This special design not only overcomes the difficulty in laser beam collimation but leads to a substantial photoacoustic enhancement > 10 owing to its strong radical resonance mode. (Fig. 18).

4. New acoustic transducer designed to improve the photoacoustic detection

4.1. The custom tuning forks

The tuning forks were invented to serve as the timekeeping element in modern clocks and smartphone in the first place in the 1960 s. Until 2002, the standard tuning forks designed for such timing applications was implemented to PAS gas sensing systems to transduce the acoustic signal into electrical signal via the piezoelectric properties of the quartz. Afterwards, various spectrophone configurations were developed based on the standard tuning forks to improve the photoacoustic detection. Although more and more tuning forks are commercially available, however most of them resonant at MHz frequency range which are not appropriate for QEPAS because the energy transfer process in gases occurs on a μs scale and the thermal wave cannot follow changes of the laser-induced excitation in the MHz range. As a result, the standard 32.768 kHz QTF is still the frequently used one in QEPAS systems reported before 2013. The above information has been reviewed in the Section 3.2. Exactly in the same year of 2013, a custom-made tuning fork was introduced to the QEPAS system, operating in the THz range with a QCL [84,85]. There are two main advantages of custom tuning forks: the first one is that the size of custom tuning forks is usually larger than the standard 32.768 kHz ones, which means the large prong spacing can extend the QEPAS to more light sources with low beam spatial qualities. This guarantees the light beam propagate through the prongs without hitting the prong-fingers, reducing the non-zero background noise from the photo-thermal effect. The second one is that the custom tuning forks are usually covered by Au film as shown in Fig. 19, in addition, different geometric structures can be custom-designed and tried to enhance the piezoelectric charge collection efficiency [85–92].

The resonant frequency of tuning fork is a very important parameter in QEPAS system, and this frequency f_0 of custom tuning forks can be designed by changing their geometric parameters as expressed in Eq.(8) [84]:

$$f_0 = \frac{\pi W}{8\sqrt{12}L^2}\sqrt{\frac{E}{\rho}}{\nu_0}^2\# \tag{7}$$

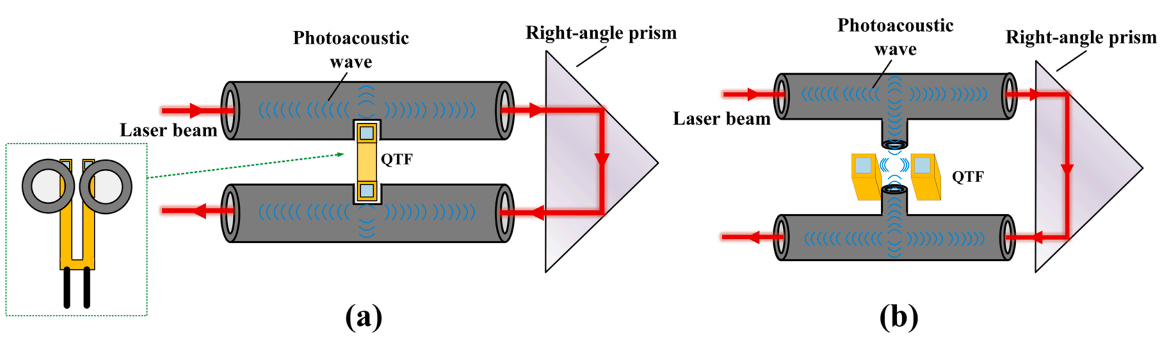

Fig. 17. Schematic of two round-trip off-beam configurations based on a right-angle prism.

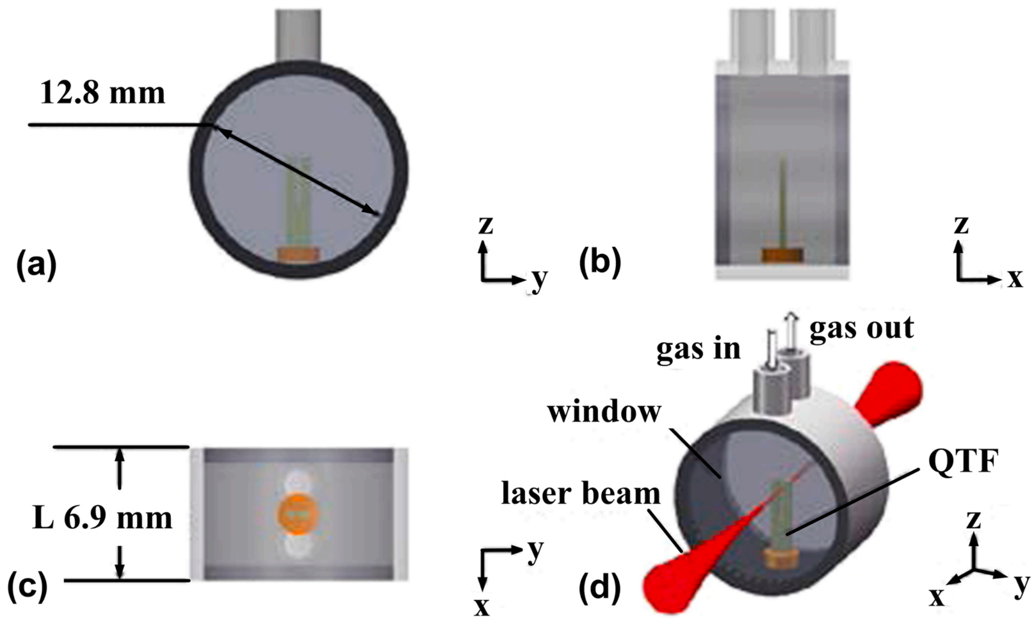

Fig. 18. Schematic diagram of radial-cavity QEPAS spectrophone. Reprinted from Ref. [83] Copyright (2021) with permission from Optical Society of America.

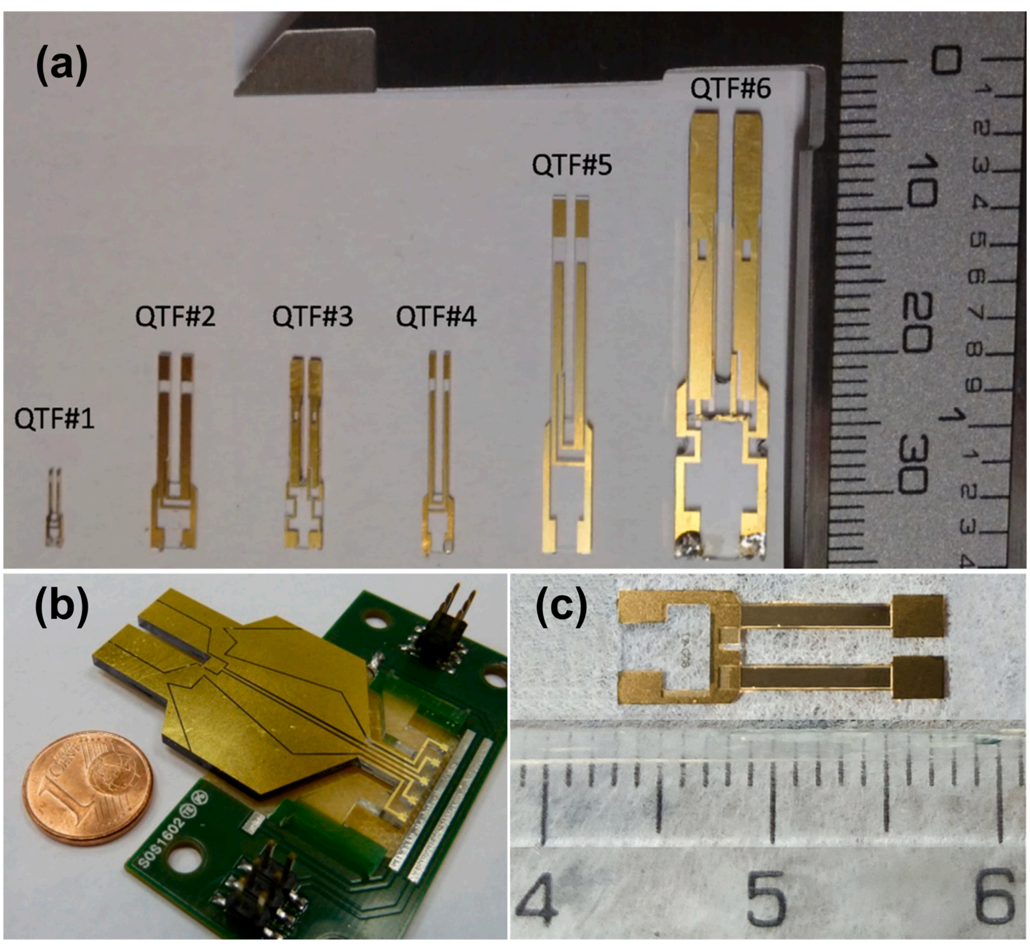

Fig. 19. Several custom QTFs developed for QEPAS gas sensing system. (a) six custom QTF in different size. Reprinted from Ref. Reprinted from an Open Access Ref. [61], (c) a T-shape custom QTF. Reprinted from Ref.
(a) [86] Copyright (2016) with permission from Elsevier, (b) a custom QTF with a 2 mm gap between the prongs. (b) [88] Copyright (2020) with permission from American Chemical Society.

where W and L are the prong thickness and length, ν_0 is 1.194 for the fundamental resonance. Based on the above theoretical model, the electro-elastic properties of several custom tuning forks as displayed in Fig. 19 (a) were analyzed and evaluated in QEPAS gas sensing system [86]. As a conclusion, lower resistance (R) and higher Q-factor are beneficial for QEPAS gas sensing system. Different sizes as shown in Fig. 19 (a) from #1 to #6 or more shapes can be optimized to satisfy different requirements for resonator frequency, resistance, Q-factor, prong spacing and so on. In 2019, Duquesnoy et al. designed a wide prong-gap QTF (2 mm) and applied it to a QEPAS CO_2 detection system. With the help of a cylindrical acoustic cavity and optimized AR, the 2 mm prong-gap QTF as shown in Fig. 19 (b) enabled the system with the CO_2 detection limit of $9 \times 10^{-9} cm^{-1}$ at 1.5μm wavelength range [61]. Recently, a T-shape tuning fork as displayed in Fig. 19 (c) was designed and applied to QEPAS system for C_2H_4, CO, N_2O detection and achieved exciting results [87–89]. As a brief summary, the custom tuning fork as a new flexible-customized acoustic transducer can directly or indirectly enhance the PA signal by its efficient piezoelectric conversion and dimensional permission for more high-power light sources and robust AR configurations [92]. In addition to the field of photoacoustic detection, tuning forks are also used as detectors in photothermal spectroscopy systems, called quartz-tuning-fork enhanced photothermal spectroscopy [90,91]. Because the photothermal spectroscopy is not the topic of this paper, so we would not carry out too much discussion.

4.2. The cantilever-based optical microphone

Condenser microphones are the most typical pressure sensors used in photoacoustic spectroscopy in the very beginning. In the condenser microphone, the vibrating element is a flexible membrane. It deforms due to the pressure variations in the surrounding gas. In order to form a capacitor with the other electrode, the membrane has to be coated with metal. The capacitance C_E varies proportionally to the pressure Δp and the displacement of the membrane Δh as [93]:

$$\Delta C_E = -\frac{\varepsilon A}{\zeta^2}\Delta\zeta \propto \Delta p \quad (\Delta\zeta \ll \zeta) \tag{8}$$

where A is the area of the electrodes and ζ is the distance between the electrodes. When the membrane vibrates due to the photoacoustic wave, it has to stretch. This causes additional damping and non-linearity to the pressure dependence of the membrane displacement. However, the cantilever is made out of silicon using a microfabrication process based on two-sided etching of silicon silicon-on-insulator wafers like pictures shown in Fig. 20. A thin cantilever moves like a saloon door induced by a pressure over the cantilever. Thus, the cantilever bends instead of stretching. Therefore, it is considerably more sensitive than the membrane to pressure vibrations. As a result, the cantilever has potential to act as a better photoacoustic transducer instead of conventional condenser microphone to improve the photoacoustic detection.

Many kinds of approaches have been proposed to measure the cantilever vibrations to calculate the photoacoustic signal when apply a cantilever to PAS gas sensing system. Among these approaches, optical method is a popular one due to its high sensitivity of optical measurement. Iris beam clipping and optical beam deflection as shown in Fig. 21 are two frequently used methods to collect the photoacoustic spectral data from the cantilever attached to the PA cell [95–97]. The Fig. 21 (a) shows a schematic illustration of an optical beam deflection method using a knife-edge detector to sense the displacement of the cantilever. In the iris beam clipping method as shown in Fig. 21 (b), an iris is used instead of the opaque screen in Fig. 21 (a) to partially block the laser beam, the function of opaque screen and iris is similar.

In addition to the above two optical methods to demodulate the cantilever displacement, optical interferometer is another high-performance choice which is usually used to detect the minor changes in the optical path. There are four famous interferometer structures: Mach-Zehnder interferometer, Sagnac interferometer, Michelson interferometer and Fabry-Perot interferometer. Among them, the Michelson interferometer (MI) and Fabry-Perot interferometer (FPI) are the most commonly used in optical coherence systems. Fig. 22 depicts a diagram of a Michelson-interferometer-based cantilever movement detector [93, 98]. The reference mirror is adjusted to make only one interference fringe cover both photodiodes $D1$ and $D2$, having a phase difference of $\pi/2$. Similarly, the photodiodes of $D3$ and $D4$ in another orthogonal branch have a phase difference of $\pi/2$. So, the optical signals reflected from different branches automatically have a phase difference of π. The voltage signals $U_1 - U_4$ and $U_2 - U_3$ are calculated as Eq. (9) and the calculated phase difference is proportional to the cantilever displacement.

$$\phi = \arctan\left(\frac{U_1 - U_4}{U_2 - U_3}\right) \tag{9}$$

If the phase exceeds 2π, the signal is calculated from the equation

$$S_n = \phi_n + 2\pi k_n, \quad k_n = -\frac{\phi_n - 2S_{n-1} + S_{n-2}}{2\pi} \tag{10}$$

k_n is rounded to the nearest integer. Compared to the beam deflection and clipping methods, the dynamic range is extended because the interference fringe continually arises after the previous one disappears.

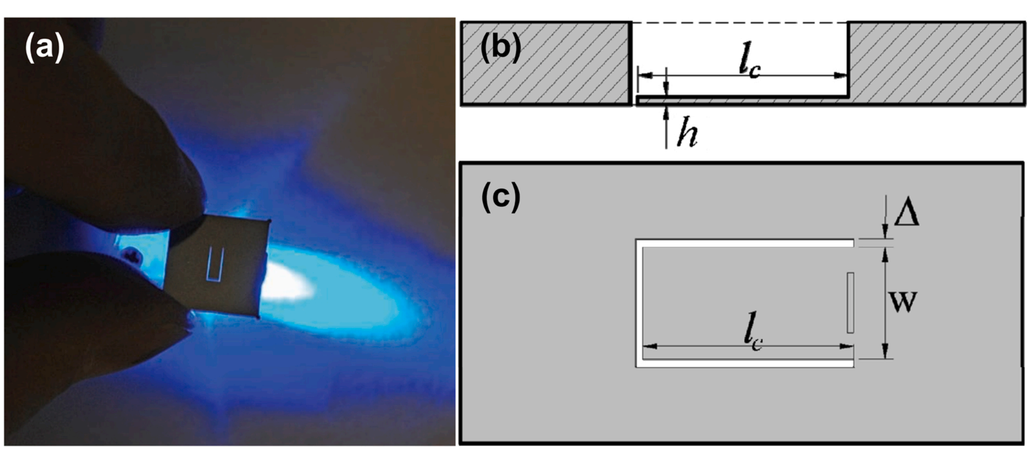

Fig. 20. (a) Silicon MEMS-fabricated cantilever pressure sensor. Reprinted from Ref. (b) The side view of frequently used cantilever, h = 10 μm, l_c = 4mm, (c) The top view, Δ = 3 ~ 5 μm, w = 1.5mm. Reprinted from Ref. thesis ISBN:978–951–29–3911–4.
(a) [94] Copyright (2021) with permission from Photonics Media. (b) [93] with permission from the author of Ph.D.

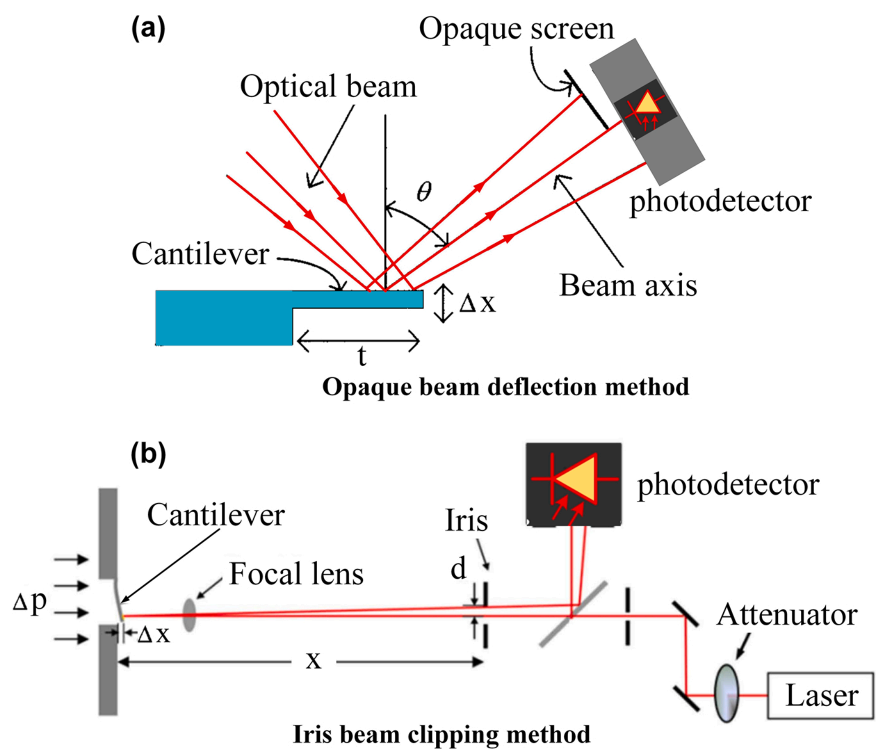

Fig. 21. Schematic illustration of opaque beam deflection method (a) and iris beam clipping method (b) to sense the cantilever displacements. Reprinted from Ref. [95] with permission from AIP Publishing and an Open Access Ref. [96].

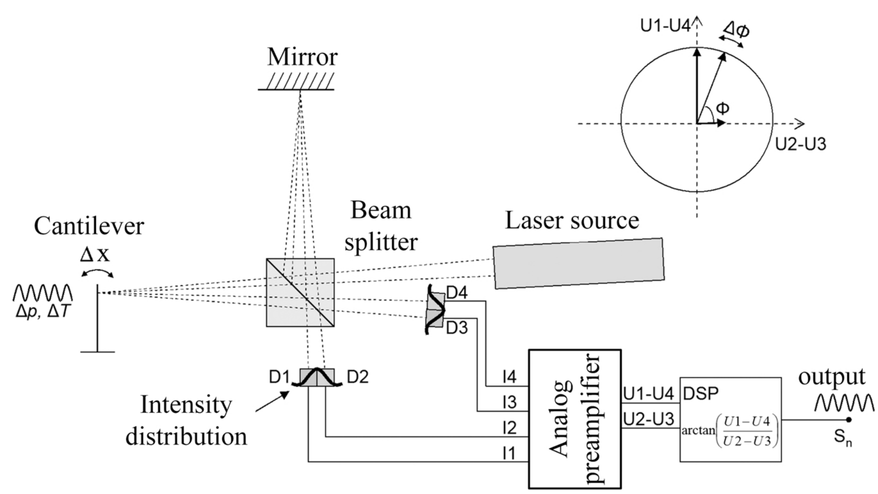

Fig. 22. Schematic illustrating an optical measurement of the cantilever movement based on Michelson type interferometer. Reprinted from Ref. [93] with permission from the author of Ph.D. thesis ISBN:978–951–29–3911–4.

The phase change of 2π corresponds to a displacement of $\lambda/2$ of the cantilever, where λ is the wavelength of the probe laser.

An example of PAS gas sensing system using the above cantilever enhanced acoustic detector is displayed in the Fig. 23, which has been developed to a commercial product "PA201". The system can be divided into two parts, one part is the fundamental photoacoustic cell for laser-gas interaction and photoacoustic excitation, a cantilever is fixed on the cell-wall; another part is a readout interferometer used to sense the vibration of cantilever. This kind of PA201 product has been applied to many cantilever-enhanced PAS systems, realizing a high sensitivity on CO, CO_2, CH_4, C_2H_2, CH_2O, HCl, HF, HCN, NO_2 detection [99–105].

Another widely used interference structure applied to sense the cantilever displacement is Fabry-Perot interferometer [106]. In 2013, Prof. Jin's group proposed a miniature fiber-tip Fabry-Perot interferometer as an acoustic sensor in the PAS gas detection, achieving an MDL of 4.3 ppm for C_2H_2 [107]. The sensor head is displayed in Fig. 24 (a), which has a polymer diaphragm to sense the photoacoustic wave realizing a minor size down to millimeter scale. The exciting light and readout laser are coupled into the same single-mode fiber (SMF), propagating to the sensor head. The photoacoustic signal is generated by the interaction between exiting light and sample gas, and then to push the diaphragm, changing the Fabry-Perot cavity length. The readout laser is used to detect the F-P cavity length. Attributed to its compact size and all-fiber configuration, this type of acoustic sensor is especially useful for space-limited and remote applications as well as largescale fiber optic sensor networks. Afterwards in 2017, researchers from Dalian University of Technology developed a high-sensitivity fiber-optic FPI based acoustic sensor with a thin silver diaphragm [108]. The silver

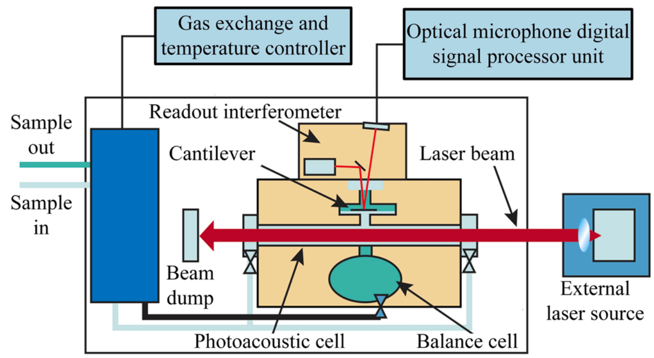

Fig. 23. Schematic of a modern cantilever-enhanced photoacoustic detector. Reprinted from Ref. [94] Copyright (2021) with permission from Photonics Media.

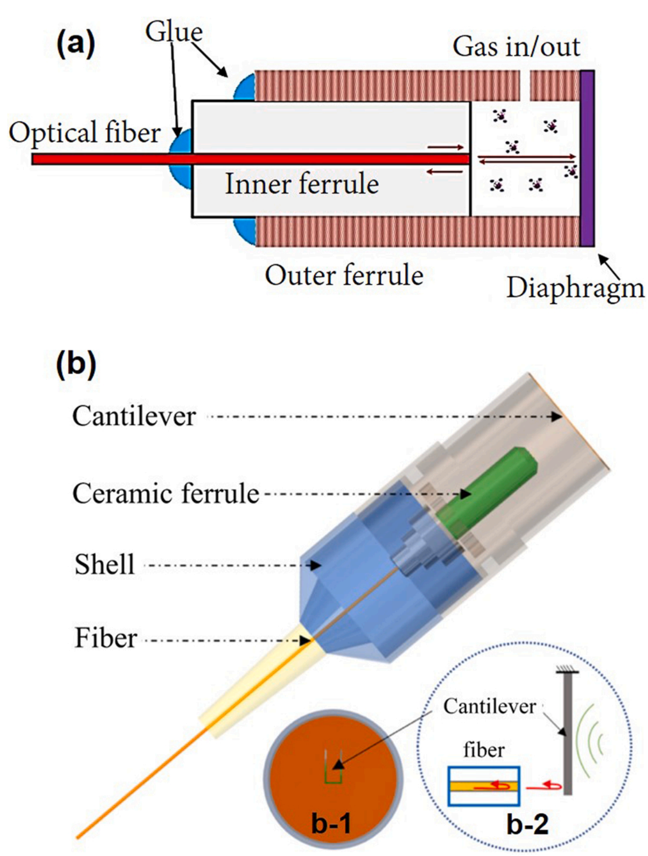

Fig. 24. (a) Schematic of the miniature fiber-tip sensor head, a FPI is formed between the fiber end and the diaphragm. (b) Diagarm of a silicon cantilever fiber-optic acoustic sensor, b-1: cantilever acoustic sensitive diaphragm, b-2: acoustic detection principle of the fiber-optic acoustic sensor. Reprinted from Ref. [109] Copyright (2022) with permission from American Chemical Society.

diaphragm has numerous advantages such as easy fabrication, strong adhesion, high pressure sensitivity and low temperature sensitivity. Moreover, thickness of the silver diaphragm is reduced to 500 nm so that the acoustic sensor has wider dynamic range and much higher pressure-sensitivity.

Considering the compact size and all-fiber characteristics of fiber-optic-based acoustic sensor, a series of efforts were made to further improve this kind of miniature all-fiber microphone. We have reviewed in the previous paragraph that a fiber-optic acoustic spectrophone can be composed by a fiber tip and a diaphragm. To overcome the nonlinear stretch as mentioned in Section 4.2, cantilever is a better choice to replace the diaphragm, making the all-fiber microphone as shown in Fig. 24 (b), the fiber end face and the cantilever serve as two surfaces of FPI. This kind of cantilever-based fiber-optic microphone is further miniaturized and has been applied to many PAS gas sensing systems. For acetylene detection, a NNEA of $10^{-10}cm^{-1}WHz^{-1/2}$ is reached in recent published studies [109–112].

Another type of miniaturized all-fiber acoustic sensor was proposed by researchers from VU University Amsterdam in 2017 [113]. A 3D sketch of the all-fiber microphone is depicted in Fig. 25 (a), an excitation fiber brings the modulated laser beam into the miniaturized PA cell which contains the sample gas to be analyzed. The photoacoustic wave generated from the gas absorption reaches the end of the PA cell, where it pushes a micro-mirror. The micro-mirror is attached to a free hanging fiber, acting the function of a cantilever. A readout fiber is aligned with the micro-mirror to detect the deflection of the cantilever induced by the photoacoustic wave. Such special-designed cantilever can reduce viscous drag losses [114]. The PA cell used in this study is very small, which is made from a capillary tube (inner diameter = 0.6 mm, outer diameter = 1 mm). Both ends are first stretched by a pipette puller and then cut and polished to proper size. As a result, the volume of sample gas within the PA cell is suppressed to 6 μL. To improve its application flexibility, a single-ended reflection configuration is developed to update the double-ended opposed type [115]. In the new configuration, the excitation fiber and readout fiber are placed side by side at the same end as shown in Fig. 25 (b) so that it can be easily inserted into various constrained spaces for in situ detection. Pushed by the continuous development of the miniaturized all-fiber acoustic sensors, an immersion PA microphone was introduced to PAS system for dissolved gas analysis successfully [116]. The immersion-style sensor head is a fiber-coupled one, and is developed on the basis of the previous configuration reported in reference [115]. The previously reported all-fiber PA microphone is fully contained in a small chamber equipped with a permeable membrane that allows dissolved gases to enter the chamber while isolating liquids outside. The immersion PA microphone is evaluated inside an oil bath to measure dissolved C_2H_2, as a result, a detection limit of 47 ppb is realized. However, the response time is measured to be as long as 180 s limited by the permeating efficiency of the membrane.

5. Discussion

Up to now, a lot of studies have been reported on the area of PAS gas detection, and more efforts are continuously paid to improve the performance of PAS systems. In this paper, representative techniques proposed to enhance the photoacoustic detection are reviewed from three aspects: (i) enhance the photoacoustic excitation, (ii) amplify the acoustic strength and (iii) develop more sensitive photoacoustic transducer. These three aspects cover the whole conducting process of a PAS system, making use of every segment related to the photoacoustic theory Eq. (2) to enhance the photoacoustic detection.

First of all, the most straightforward method to enhance the photoacoustic excitation is utilizing high-power laser source. The process of photoacoustic excitation is similar to beating a drum with a stick, merely the special "stick" in PAS system is the laser beam to be absorbed by the gas molecule. Thus, "beating the drum harder" in PAS system will be certain to make the photoacoustic signal louder. In the photoacoustic generation, the process of photons-molecules interaction plays the role of the special "stick" and both increasing the optical power and molecules absorption can make the "stick" heavier to obtain a louder photoacoustic signal. Considering that the degree of molecules absorption depends on its line strength, which is decided by the specific structure of molecule's energy level, therefore, increasing optical power becomes the most straightforward choice to enhance the "drum stick". The Table 1 lists several representative studies to enhance the photoacoustic excitation by virtue of increasing the optical power, among them the simplest approach is searching for some special lasers with high power

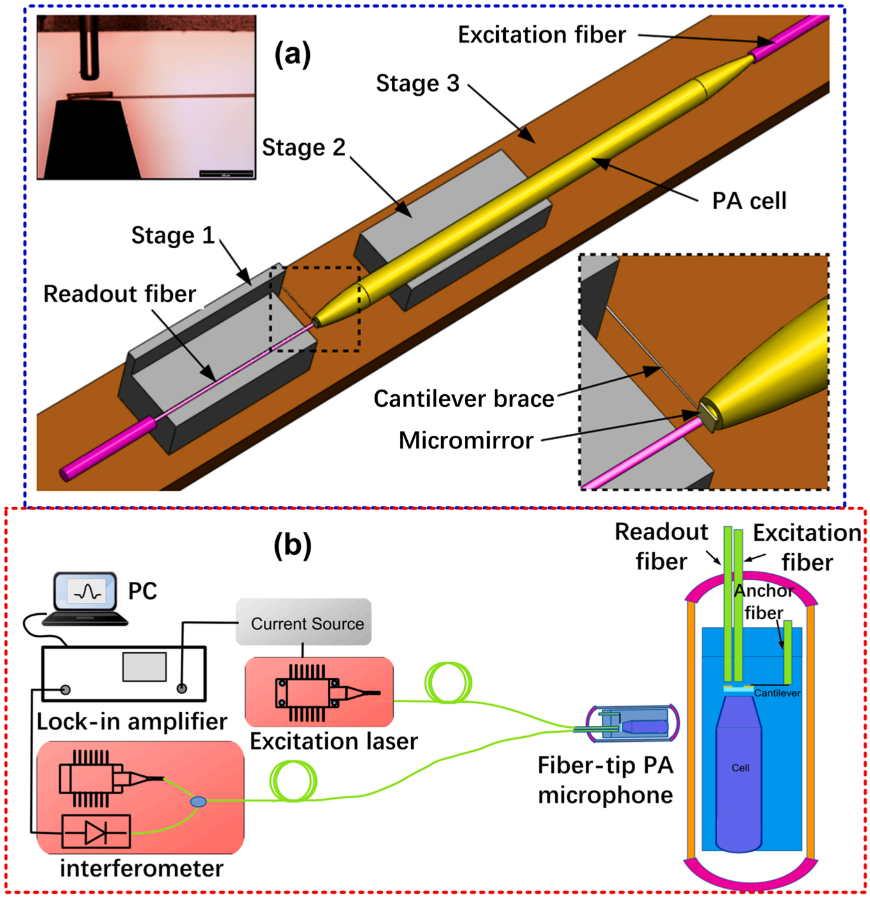

Fig. 25. (a) 3D sketch of manufacturing a miniaturized all-fiber microphone. Insets: enlarged sketch and microscopic views of the micro-mirror alignment against the PA cell and the readout fiber. (b) PAS system utilizing this kind of miniaturized all-optical microphone. Right side: detailed view of the fiber-tip PA microphone. Reprinted from an Open Access Ref. [113] Copyright (2017) Optical Society of America.

output. However, this approach is very limited because there is no guarantee that high-power lasers are always available at any desirable wavelength region. Compared to selecting a high-power laser source directly, EDFA is adopted to amplify the seed laser operating at 1500 nm band, which is applied to many PAS systems for H_2S, C_2H_2 and NH_3 detection. In addition, our group members are focusing on developing Tm-doped fiber amplifier (TDFA) to improve the CO_2 photoacoustic detection at 2000 nm band. However, the EDFA or TDFA still has limitations because it only applies to a specific spectral region limited by the doped ion. Afterwards, the extra-cavity enhanced PAS and intra-cavity enhanced PAS are proposed, in which laser power is built up inside the cavity and PA cell is inserted to the cavity to make use of the accumulated laser power. Theoretically, this method is more compatible with different wavelengths as long as the corresponding cavity mirrors are available. Furthermore, the Q-switch technique can be introduced to PAS systems to obtain high-power laser pulse if PA cell was inserted inside the laser resonant cavity successfully.

Secondly, strategies are proposed to enlarge the acoustic strength after the process of photoacoustic excitation. A unified direction is to design a resonant PA cell inside which a strong and stable standing wave field is formed. Thus, an enhanced photoacoustic signal can be captured to calculate the absorption. For example, different Helmholtz PA cells are designed for this purpose. However, a common disadvantage of this kind PA cell is the low-Q-factor. So, more attention is focused on how to amplify the acoustic wave in QEPAS gas sensing system. Various micro-resonators are made and assembled to generate and amplify the standing wave field as compared in Table 2, which can be divided into two types, on-beam structure and off-beam structure. The advantages of the on-beam structure include that the micro resonant tubes are easily manufactured, the dimensional parameters of resonant tubes are easily optimized and low acoustic energy loss is easily realized. Moreover, the photoacoustic gain factor can reach two decades based on a single-tube on-beam configuration [66,67]. However, high-quality optical alignment remains challenging because of that the laser beam should not only pass through the resonant tubes but also the gap of QTF prongs. Considering the gap space of the most commonly used 32.768 kHz QTF is only 0.3 mm, so the optical alignment must be strictly operated without touching resonant tubes or QTF prongs. Of course, custom tuning fork with large prong gap can relieve the difficulties from the prong gap limitation. In addition, the off-beam structure is another alternative configuration for easier optical alignment, in which the resonant tube is placed parallel to the QTF so that laser beam just needs to pass through the tube hole. Photoacoustic energy escapes from a slit cut in the middle of the resonant tube to push the QTF prongs. Compared with the on-beam structure, more dimensional parameters should be carefully designed for off-beam resonant tubes in addition to the tube length and inner diameter. For example, the slit length and width directly determine the acoustic coupling efficiency between resonator and QTF. For the T-shape resonator used in off-beam configuration, the length and inner diameter of T-branch are also very critical for photoacoustic enhancement [80]. As to the gain factor, it is hard to say which structure, on-beam or off beam, is the better one in our opinion if their optimal parameters have been realized.

Lastly, an acoustic transducer is employed to sense the photoacoustic wave after the excitation and amplification process. In the earliest PAS system, electric microphones are mounted to the PA cell to detect the photoacoustic signal. Limited by the low resonant frequency of PA cell and sensitivity of electric microphones, it is very difficult to achieve high

Table 1
Different strategies used to enhance the photoacoustic excitation by using high-power laser sources or amplifying the optical power. EDFA: erbium doped fiber amplifier, EC-PAS: extra-cavity enhanced photoacoustic spectroscopy, FLI-PAS: fiber laser intra-cavity photoacoustic spectroscopy, FLI-QEPAS: fiber laser intra-cavity quartz enhanced photoacoustic spectroscopy, MDL: minimum detection limit, Effective Optical Power: the ultimate optical power excites the photo-acoustic signal.

Method of Photoacoustic Excitation	Gas	Wavelength	Effective Optical Power	MDL	Ref.
High-power light source	$^{14}CH_4$	3 μm	95 mW	83 ppb @ 12 min	[16]
	NO_2	447 nm	3.5 W	54 ppt @ 1 s	[19]
EDFA	H_2S	1582 nm	1.36 W	109 ppb @ 1 s	[23]
	C_2H_2	1531.6 nm	1 W	0.37 ppb @ 60 s	[24]
	H_2S	1582 nm	1.4 W	142 ppb @ 67 s	[25]
	NH_3	1531 nm	1 W	418.4 ppb @ 1 s	[27]
	C_2H_2	1530.3 nm	1.5 W	33.2 ppb @ 1 s	[28]
EC-PAS	H_2O	10.4 μm	9.6 W	< 10 ppb	[35]
	H_2O	635 nm	2.5 W	4.4×10^{-9} $cm^{-1}/\sqrt{Hz}$ @ 1 s	[2]
	CO_2	4.33 μm	0.75 W	300ppt @ 4 s	[17]
	C_2H_2	1530.3 nm	1 W	8.17 ppb @ 1 s	[32]
FLI-PAS/FLI-QEPAS	C_2H_2	1531.6 nm	108 mW	390 ppb @ 2 s	[15]
	C_2H_2	1531.6 nm	460 mW	29 ppb @ 300 s	[43]
	C_2H_2	1530.3 nm	6 W	101 ppt @ 20 ms	[47]
	C_2H_2	1532.8 nm	0.88 W	32 ppb @ 268 s	[48]
	C_2H_2	1531.6 nm	3 W	26 ppb @ 50 ms	[49]

Table 2
Different acoustic resonant configurations used in QEPAS system. Gain Factor: the photoacoustic enhancement factor compared to the bare QTF operating in the fundamental resonant mode.

Type	Arrangement of Micro-resonators	Operating Frequency	Gain Factor	Ref.
On Beam	single-beam dual-tubes	32.7 kHz	30	[64]
	single-beam half-tube	32.7 kHz	21	[62]
	single-beam single-tube	7.2 kHz	128	[66]
	single-beam single-tube	17.7 kHz	380	[67]
	dual-beams four-tubes	32.7 kHz	22.4	[71]
	multiple-beams without resonators	7.2 kHz	20	[72]
Off Beam	single-beam single-tube (parallel mode)	32.7 kHz	15.7	[74]
	single-beam single-tube (inserted mode)	32.7 kHz	25	[78]
	dual-beams dual-tubes (inserted mode)	32.7 kHz	40	[78]
	T-shape	32.7 kHz	30	[80]
	H-shape	32.7 kHz	17.2	[82]
	radial-cavity	32.7 kHz	11.3	[83]

Q-factor based on this kind of combination. Afterwards in 2002, the QEPAS technique was first proposed by Kosterev et al. and QTF was used as an alternative device to detect weak PA signal [58]. Usually, QEPAS system comprises commercially available piezoelectric QTF as transducers converting acoustic wave to electric signal efficiently. To further increase the acoustic detection sensitivity and permit more resonant structures, various custom tuning forks have been developed as list in Table 3. The size of custom tuning forks is usually larger than the commercial one, which means the large prong gap can extend the QEPAS to more light sources with lower beam spatial quality. This guarantees the light beam propagate through the prong gap without hitting the prong itself, reducing the non-zero background noise from the photo-thermal effect. In addition, researchers try to electroplate the tuning forks' surface with aurum to enhance the piezoelectric charge collection efficiency. As a result, NNEA as low as 10^{-11} $cm^{-1}WHz^{-1/2}$ is realized by virtue of this kind of custom tuning fork. Another ultra-sensitive acoustic detector is micro cantilever, and among lots of approaches to measure the cantilever vibrations, optical interferometer is an advanced one due to the high sensitivity of optical interference. What's more exciting in this part is the creative fiber tip microphone, in which F-P cavity is formed between the fiber end face and cantilever surface. Thus, this kind of all-fiber microphone can be designed to a super miniaturization, applied to cramped places with limited space. Meanwhile, the F-P interferometer-based fiber tip microphone has ability of anti-electromagnetic interference. Given by the published results utilizing this kind of fiber tip microphone as shown in Table 3, a NNEA of 10^{-10} $cm^{-1}WHz^{-1/2}$ can be achieved, which reaches the same level of a commercial cantilever-based microphone (PA201).

From the day when PAS technique was introduced to gas sensing, researchers have paid a lot of attention on this field. Compared with the direct absorption spectroscopy, PAS technique really has its unique advantages as below:

- ✓ PAS system does not require an optical detector. Therefore, it has no selectivity for operating wavelength so that it can be applied to all wavelength from ultra-violet to terahertz.
- ✓ The photoacoustic signal scales with absorbed power, high-power lasers directly increase the photoacoustic excitation.
- ✓ PAS is a baseline-free technique where the absorbed energy is measured, rather than the strong transmitted radiation background as in TDLAS, which means the dynamic range of pre-amplifier circuits can be fully exploited.

Until now, PAS is still a research hotspot. In addition to the above advantages coming from its operating mechanism, PAS-based gas sensor also has superiority in specific application environment. For example, the PAS-based gas sensor can be applied to narrow space measurement because of its little gas consumption and independence on absorption path length. Another example in reference [116], an all-fiber microphone is fully contained in a small chamber equipped with a permeable membrane, opening the gate for the PAS system to sense the dissolved gases without degassing operation. This is an anticipated potential that expanding the PAS technique to in-situ detection in liquid. As an indirect absorption-based gas sensing technique, we can see that PAS has great potential which deserves for more effort. We expect several prospects to further push the PAS-related technologies into reality in the further as: (i) Develop more sensitive acoustic transducer such as new generation of QTF and fiber-optic microphone. (ii) Develop ultra-compact intra-cavity PAS sensor for high-sensitive detection. (iii) Push PAS sensing systems development for real-world application and commercialization, for example the downhole petrochemical applications, breath diagnosis, airborne-based environmental monitoring.

6. Conclusion

In conclusion, this paper is a comprehensive review from the perspective of photoacoustic enhancement. We believe most of the photoacoustic enhanced techniques so far have been reviewed here. We hope this review together with the full discussion on the principles, experimental results, advantages, and disadvantages of each photo-acoustic enhanced strategy could offer necessary help as a handbook for researchers with strong motivations to improve their PAS system detection limitation. Honestly, it is hard and unfair to judge which

Table 3
Different developed acoustic detector designed to improve the photoacoustic detection. Dimension: length×width×thickness, PG: prong gap, λ: operating wavelength, MDL: minimum detection limit, NNEA: normalized noise equivalent absorption coefficient.

Type	Dimension	PG	Gas	λ	MDL	NNEA	Ref.
Custom Tuning Fork	33 mm × 4 mm× 0.8 mm	0.8 mm	CH_4O	76.3 µm	7 ppm @ 4 s	2×10^{-10} cm^{-1}WHz$^{-1/2}$	[85]
	9.4 mm × 2 mm× 0.8 mm	0.8 mm	C_2H_4	10.3 µm	10ppb @ 10 s	\	[87]
	13.6 mm × 8 mm× 2 mm	2.0 mm	CO_2	1.54 µm	44 ppm @ 19 min	3.7×10^{-9} cm^{-1}WHz$^{-1/2}$	[61]
	12.6 mm × 4.8 mm× 0.25 mm	0.8 mm	CO	4.61 µm	90ppb @ 1 s	1.8×10^{-7} cm^{-1}WHz$^{-1/2}$	[88]
	12.6 mm × 4.8 mm× 0.25 mm	0.8 mm	CO	4.59 µm	260ppt @ 10 s	3.8×10^{-10} cm^{-1}WHz$^{-1/2}$	[89]
			N_2O		750ppt @ 10 s	1.7×10^{-10} cm^{-1}WHz$^{-1/2}$	
			H_2O		5.9 ppm @ 10 s	1.9×10^{-11} cm^{-1}WHz$^{-1/2}$	
	3.3 mm × 1 mm× 0.35 mm	0.2 mm	H_2O	1389.9 nm	6.3 ppm @ 84 s	1.7×10^{-8} cm^{-1}WHz$^{-1/2}$	[92]
Type			**Gas**	**λ**	**MDL**	**NNEA**	**Ref.**
Cantilever-based Microphone (PA201)			CH_2O	5.6 µm	1.3 ppb @ 1 s	6.0×10^{-10} cm^{-1}WHz$^{-1/2}$	[99]
			HF	2475.9 nm	650ppq @ 32 min	2.7×10^{-10} cm^{-1}WHz$^{-1/2}$	[101]
			$^{14}CO_2$	4.5 µm	30ppt @ 9 min	8×10^{-9} cm^{-1}WHz$^{-1/2}$	[102]
			NO_2	532 nm	50ppt @ 1 s	2.6×10^{-10} cm^{-1}WHz$^{-1/2}$	[103]
			HCN	3 µm	190ppt @ 1 s	1.8×10^{-9} cm^{-1}WHz$^{-1/2}$	[104]
			CH_4	3.27 µm	65ppt @ 30 s		
Cantilever-based Microphone (F-P cavity based miniature fiber-tip acoustic sensor)			C_2H_2	1.53 µm	4.3 ppm @ 10 s	\	[107]
			C_2H_2	1531.6 nm	0.87ppb @ 0.1 s	\	[108]
			C_2H_2	1532.8 nm	1.51ppb @ 1 s	1.7×10^{-9} cm^{-1}WHz$^{-1/2}$	[109]
			C_2H_2	1532.8 nm	27ppt @ 200 s	4.2×10^{-10} cm^{-1}WHz$^{-1/2}$	[111]
			CH_4	1650.9 nm	8.4 ppm @ 1 s	2.1×10^{-8} cm^{-1}WHz$^{-1/2}$	[112]
			C_2H_2	1530.5 nm	15ppb @ 0.3 s	7.7×10^{-10} cm^{-1}WHz$^{-1/2}$	[113]

technique is the best choice without considering the specific applications. There is not an omnipotent technique to satisfy every requirement, but we can make the best strategy against a certain application by stepping on the shoulders of all published technologies.

Funding

National Natural Science Foundation of China (52001295, 62005267, 41575023, U2006209), Natural Science Foundation of Shandong Province (ZR2020QF097, ZR2021QD140), Open Fund of State Key Laboratory of Applied Optics (SKLAO2021001A12), Key Research and Development Program of Shandong Province (2020CXGC010706), Key project of major subject of new and old kinetic energy conversion in Shandong Province (2020XJDN010039), Fundamental Research Funds for the Central Universities (202013024, 202065004), Shandong Postdoctoral Innovation Program.

Declaration of Competing Interest

The authors declare that they have no known competing financial interests or personal relationships that could have appeared to influence the work reported in this paper.

Data availability

No data was used for the research described in the article.

References

[1] P. Patimisco, G. Scamarcio, F.K. Tittel, V. Spagnolo, Quartz-enhanced photoacoustic spectroscopy: a review, Sensors 14 (2014) 6165–6206.
[2] M. Hippler, C. Mohr, K.A. Keen, E.D. McNaghten, Cavity-enhanced resonant photoacoustic spectroscopy with optical feedback cw diode lasers: a novel technique for ultratrace gas analysis and high-resolution spectroscopy, J. Chem. Phys. 133 (2010), 044308.
[3] E.D. Hinkley, High–resolution infrared spectroscopy with a tunable diode laser, Appl. Phys. Lett. 16 (1970) 351–354.
[4] M. Loewenstein, Diode laser harmonic spectroscopy applied to in situ measurements of atmospheric trace molecules, J. Quant. Spectrosc. Radiat. Transf. 40 (1988) 249–256.
[5] J. Reid, B.K. Garside, J. Shewchun, M. El-Sherbiny, E.A. Ballik, High sensitivity point monitoring of atmospheric gases employing tunable diode lasers, Appl. Opt. 17 (1978) 1806–1810.
[6] A.G. Bell, On the production and reproduction of sound by light, J. Soc. Telegr. Eng. 9 (34) (1880) 404–426.
[7] T. Yang, W. Chen, P. Wang, A review of all-optical photoacoustic spectroscopy as a gas sensing method, Appl. Spectrosc. Rev. 56 (2021) 143–170.
[8] A. Sampaolo, P. Patimisco, M. Giglio, A. Zifarelli, H. Wu, L. Dong, V. Spagnolo, Quartz-enhanced photoacoustic spectroscopy for multi-gas detection: a review, Anal. Chim. Acta (2021), 338894.
[9] V. Spagnolo, P. Patimisco, S. Borri, A. Sampaolo, G. Scamarcio, M.S. Vitiello, H. E. Beere, D.A. Ritchie, THz quartz-enhanced photoacoustic sensor employing a quantum cascade laser source, in: Quant. Sens. Nanophotonic Devices XI, 8993, SPIE,, 2014, pp. 309–319.
[10] V. Spagnolo, P. Patimisco, A. Sampaolo, M. Giglio, M.S. Vitiello, G. Scamarcio, F. K. Tittel, New developments in THz quartz enhanced photoacoustic spectroscopy, Terahertz Emitters, in: Receivers, and Applications VII, 9934, SPIE,, 2016, pp. 43–50.
[11] M. Mordmueller, W. Schade, U. Willer, QEPAS with electrical co-excitation for photoacoustic measurements in fluctuating background gases, Appl. Phys. B 123 (2017) 224.
[12] P. Werle, Accuracy and precision of laser spectrometers for trace gas sensing in the presence of optical fringes and atmospheric turbulence, Appl. Phys. B 102 (2011) 313–329.
[13] A. Miklós, P. Hess, Z. Bozóki, Application of acoustic resonators in photoacoustic trace gas analysis and metrology, Rev. Sci. Instrum. 72 (2001) 1937–1955.
[14] A. Elia, P.M. Lugarà, C. Di Franco, V. Spagnolo, Photoacoustic techniques for trace gas sensing based on semiconductor laser sources, Sensors 9 (12) (2009) 9616–9628.
[15] Q. Wang, Z. Wang, J. Chang, W. Ren, Fiber-ring laser-based intracavity photoacoustic spectroscopy for trace gas sensing, Opt. Lett. 42 (2017) 2114–2117.
[16] Juho Karhu, Teemu Tomberg, Francisco Senna Vieira, Guillaume Genoud, Vesa Hanninen, Markku Vainio, Markus Metsala, Tuomas Hieta, Steven Bell, Lauri Halonen, Broadband photoacoustic spectroscopy of $^{14}CH_4$ with a high-power mid-infrared optical frequency comb, Opt. Lett. 44 (2019) 1142–1145.
[17] S. Borri, P. Patimisco, I. Galli, D. Mazzotti, G. Giusfredi, N. Akikusa, M. Yamanishi, G. Scamarcio, P. De Natale, V. Spagnolo, Intracavity quartz-enhanced photoacoustic sensor, Appl. Phys. Lett. 104 (2014), 091114.
[18] Y. Ma, R. Lewicki, M. Razeghi, F.K. Tittel, QEPAS based ppb-level detection of CO and N_2O using a high power CW DFB-QCL, Opt. Express 21 (1) (2013) 1008.
[19] A. Pourhashemi, R.M. Farrell, D.A. Cohen, J.S. Speck, S.P. DenBaars, S. Nakamura, High-power blue laser diodes with indium tin oxide cladding on semipolar GaN substrates, Appl. Phys. Lett. 106 (2015), 111105.
[20] X. Yin, L. Dong, H. Wu, H. Zheng, W. Ma, L. Zhang, W. Yin, S. Jia, F.K. Tittel, Sub-ppb nitrogen dioxide detection with a large linear dynamic range by use of a differential photoacoustic cell and a 3.5W blue multimode diode laser, Sens. Actuators B-Chem. 247 (2017) 329–335.
[21] P.M. Becker, A.A. Olsson, J.R. Simpson, Erbium-doped fiber amplifiers: fundamentals and technology. CA, Academic Press, San Diego, 1999.
[22] M.E. Webber, M. Pushkarsky, C.K.N. Patel, Fiber-amplifier-enhanced photoacoustic spectroscopy with near-infrared tunable diode lasers, Appl. Opt. 42 (2003) 2119–2126.
[23] X. Yin, L. Dong, H. Wu, W. Ma, L. Zhang, W. Yin, L. Xiao, S. Jia, F.K. Tittel, Ppb-level H2S detection for SF6 decomposition based on a fiber-amplified telecommunication diode laser and a background-gas-induced high-Q photoacoustic cell, Appl. Phys. Lett. 111 (2017), 031109.
[24] K. Chen, Z. Gong, Q. Yu, Fiber-amplifier-enhanced resonant photoacoustic sensor for sub-ppb level acetylene detection, Sens. Actuators A-Phys. 274 (2018) 184–188.
[25] H. Wu, L. Dong, H. Zheng, X. Liu, X. Yin, W. Ma, L. Zhang, W. Yin, S. Jia, F. K. Tittel, Enhanced near-infrared QEPAS sensor for sub-ppm level H2S detection

by means of a fiber amplified 1582nm DFB laser, Sens. Actuators B-Chem. 221 (2015) 666–672.
[26] Y. He, Y. Ma, Y. Tong, X. Yu, Z. Peng, J. Gao, F.K. Tittel, Long distance, distributed gas sensing based on micro-nano fiber evanescent wave quartz-enhanced photoacoustic spectroscopy, Appl. Phys. Lett. 111 (2017), 241102.
[27] Y. Ma, Y. He, Y. Tong, X. Yu, F.K. Tittel, Ppb-level detection of ammonia based on QEPAS using a power amplified laser and a low resonance frequency quartz tuning fork, Opt. Express 25 (2017) 29356–29364.
[28] Y. Ma, Y. He, L. Zhang, X. Yu, J. Zhang, R. Sun, F.K. Tittel, Ultra-high sensitive acetylene detection using quartz-enhanced photoacoustic spectroscopy with a fiber amplified diode laser and a 30.72 kHz quartz tuning fork, Appl. Phys. Lett. 110 (2017), 031107.
[29] K. Song, S. Oh, E.C. Jung, D. Kim, H. Cha, Application of laser photoacoustic spectroscopy for the detection of water vapor near 1.38 μm, Microchem. J. 80 (2005) 113–119.
[30] Y. Pan, L. Dong, H. Wu, W. Ma, L. Zhang, W. Yin, L. Xiao, S. Jia, F.K. Tittel, Cavity-enhanced photoacoustic sensor based on a whispering-gallery-mode diode laser, Atmos. Meas. Tech. 12 (2019) 1905–1911.
[31] L. Hao, S. Qiang, G. Wu, L. Qi, D. Feng, Q. Zhu, Z. Hong, Cylindrical mirror multipass Lissajous system for laser photoacoustic spectroscopy, Rev. Sci. Instrum. 73 (2002) 2079.
[32] Y. Ma, S. Qiao, Y. He, Y. Li, Z. Zhang, X. Yu, F.K. Tittel, Highly sensitive acetylene detection based on multi-pass retro-reflection-cavity-enhanced photoacoustic spectroscopy and a fiber amplified diode laser, Opt. Express 27 (2019) 14163–14172.
[33] Y. Ma, H. Dang, Corner cube prism-enhanced photoacoustic spectroscopy based gas sensing, Infrared Phys. Technol. 109 (2020), 103386.
[34] A. Rossi, R. Buffa, M. Scotoni, D. Bassi, S. Iannotta, A. Boschetti, Optical enhancement of diode laser-photoacoustic trace gas detection by means of external Fabry-Perot cavity, Appl. Phys. Lett. 87 (2005), 041110.
[35] A. Kachanov, S. Koulikov, F.K. Tittel, Cavity-enhanced optical feedback-assisted photo-acoustic spectroscopy with a 10.4 μm external cavity quantum cascade laser, Appl. Phys. B 110 (2013) 47–56.
[36] P. Patimisco, S. Borri, I. Galli, D. Mazzotti, G. Giusfredi, N. Akikusa, M. Yamanishi, G. Scamarcio, P.D. Nataleb, V. Spagnolo, High finesse optical cavity coupled with a quartz-enhanced photoacoustic spectroscopic sensor, Analyst 140 (2015) 736–743.
[37] W. Jacek, G. Aleksander, H. Arkadiusz, F.K.Tittel Mid-Infrared, Trace gas sensor technology based on intracavity quartz-enhanced photoacoustic spectroscopy, Sensors 17 (3) (2017).
[38] Z. Wang, Q. Wang, W. Zhang, H. Wei, Y. Li, W. Ren, Ultrasensitive photoacoustic detection in a high-finesse cavity with Pound-Drever-Hall locking, Opt. Lett. 44 (8) (2019) 1924–1927.
[39] J. Röper, G. Chen, P. Hess, Intracavity photoacoustic resonance spectroscopy of C2H4, Appl. Phys. B 43 (1987) 57–59.
[40] Z. Bozóki, J. Sneider, G. Szabó, A. Miklós, M. Serényi, G. Nagy, M. Fehér, Intracavity photoacoustic gas detection with an external cavity diode laser, Appl. Phys. B 63 (1996) 399–401.
[41] V.S. Starovoitov, J.F. Kischkat, M.P. Semtsiv, W.T. Masselink, Intracavity photoacoustic sensing of water vapor with a continuously tunable external-cavity quantum-cascade laser operating near 5.5 μm, Opt. Lett. 41 (2016) 4955–4958.
[42] P. Dupriez, A. Piper, A. Malinowski, J.K. Sahu, M. Ibsen, B.C. Thomsen, Y. Jeong, L.M.B. Hickey, M.N. Zervas, J. Nilsson, D.J. Richardson, High average power, high repetition rate, picosecond pulsed fiber master oscillator power amplifier source seeded by a gain-switched laser diode at 1060 nm, IEEE Photonics Technol. Lett. 18 (2006) 1013–1015.
[43] Q. Wang, Z. Wang, W. Ren, P. Patimisco, A. Sampaolo, V. Spagnolo, Fiber-ring laser intracavity QEPAS gas sensor using a 7.2 kHz quartz tuning fork, Sens. Actuators B-Chem. 268 (2018) 512–518.
[44] Z. Luo, M. Zhou, J. Weng, G. Huang, H. Xu, C. Ye, Z. Cai, Graphene-based passively Q-switched dual-wavelength erbium-doped fiber laser, Opt. Lett. 35 (2010) 3709–3711.
[45] N.A. Russo, R. Duchowicz, J. Mora, J.L. Cruz, M.V. Andrés, High-efficiency Q-switched erbium fiber laser using a Bragg grating-based modulator, Opt. Commun. 210 (2002) 361–366.
[46] M. Delgado-Pinar, D. Zalvidea, A. Díez, P. Pérez-Millán, M.V. Andrés, Q-switching of an all-fiber laser by acousto-optic modulation of a fiber Bragg grating, Opt. Express 14 (2006) 1106–1112.
[47] Q. Zhang, J. Chang, Z. Cong, Y. Feng, Z. Wang, F. Wang, J. Sun, Pptv-level intra-cavity QEPAS sensor for acetylene detection using a high power Q-switched fiber laser, IEEE Sens. J. 19 (2019) 6181–6186.
[48] Q. Zhang, J. Chang, Z. Cong, Y. Feng, Z. Wang, J. Sun, Scanned-wavelength intra-cavity QEPAS sensor with injection seeding technique for C2H2 detection, Opt. Laser Technol. 120 (2019), 105751.
[49] F. Wang, Q. Xue, J. Chang, Z. Wang, J. Sun, X. Luan, C. Li, Wavelength scanning Q-switched fiber-ring laser intra-cavity QEPAS using a standard 32.76 kHz quartz tuning fork for acetylene detection, Opt. Laser Technol. 134 (2021), 106612.
[50] M. Pollnau, S.D. Jackson, Mid-Infrared Fiber Lasers, in: I.T. Sorokina, K.L. Vodopyanov (Eds.), Solid-State Mid-Infrared Laser Sources, Springer, Berlin, Heidelberg, 2003, pp. 225–261.
[51] B. Debord, F. Amrani, L. Vincetti, F. Gérôme, F. Benabid, Hollow-core fiber technology: the rising of "Gas Photonics, Fibers 7 (2019) 16.
[52] P.M. Morse, K.U. Ingard, Theoretical Acoustics, Princeton University Press, Princeton, 1986.
[53] L.E. Kinsley, A.R. Frey, A.B. Coppens, J.V. Sanders, Fundamentals of Acoustics, Wiley, New York, 1982.
[54] M. Fiedler, P. Hess, Laser Excitation of Acoustic Modes in Cylindrical and Spherical Resonators: Theory and Applications, in: P. Hess (Ed.), Photoacoustic, Photothermal and Photochemical Processes in Gases, Springer, Berlin, Heidelberg, 1989, pp. 85–123.
[56] Z. Gong, T. Gao, L. Mei, K. Chen, Y. Chen, B. Zhang, W. Peng, Q. Yu, Ppb-level detection of methane based on an optimized T-type photoacoustic cell and a NIR diode laser, Photoacoustics 21 (2021), 100216.
[57] Z. Gong, G. Wu, X. Jiang, H. Li, T. Gao, M. Guo, F. Ma, K. Chen, L. Mei, W. Peng, Q. Yu, All-optical high-sensitivity resonant photoacoustic sensor for remote CH4 gas detection, Opt. Express 29 (2021) 13600–13609.
[58] A.A. Kosterev, Y.A. Bakhirkin, R.F. Curl, F.K. Tittel, Quartz-enhanced photoacoustic spectroscopy, Opt. Lett. 27 (2002) 1902–1904.
[59] H. Wu, A. Sampaolo, L. Dong, P. Patimisco, X. Liu, H. Zheng, X. Yin, W. Ma, L. Zhang, W. Yin, V. Spagnolo, S. Jia, F.K. Tittel, Quartz enhanced photoacoustic H2S gas sensor based on a fiber-amplifier source and a custom tuning fork with large prong spacing, Appl. Phys. Lett. 107 (2015), 111104.
[60] P. Patimisco, S. Borri, A. Sampaolo, H.E. Beere, D.A. Ritchie, M.S. Vitiello, G. Scamarcio, V. Spagnolo, A quartz enhanced photo-acoustic gas sensor based on a custom tuning fork and a terahertz quantum cascade laser, Analyst 13 (2014) 2079–2087.
[61] M. Duquesnoy, G. Aoust, J.M. Melkonian, R. Lévy, M. Raybaut, A. Godard, Quartz enhanced photoacoustic spectroscopy based on a custom quartz tuning fork, Sensors 19 (2019) 1362.
[62] H. Yi, W. Chen, X. Guo, S. Sun, K. Liu, T. Tan, W. Zhang, X. Gao, An acoustic model for microresonator in on-beam quartz-enhanced photoacoustic spectroscopy, Appl. Phys. B 108 (2012) 361–367.
[63] F. Wang, J. Chang, Q. Zhang, Z. Qin, C. Zhu, Pivotal techniques evaluation in QEPAS system for engineering applications, Measurement 135 (2019) 376–384.
[64] L. Dong, A.A. Kosterev, D. Thomazy, F.K. Tittel, QEPAS spectrophones: design, optimization, and performance, Appl. Phys. B 100 (2010) 627–635.
[65] Y. Cao, W. Jin, H.L. Ho, Optimization of spectrophone performance for quartz-enhanced photoacoustic spectroscopy, Sens. Actuators B-Chem. 174 (2012) 24–30.
[66] H. Zheng, L. Dong, A. Sampaolo, H. Wu, P. Patimisco, X. Yin, W. Ma, L. Zhang, W. Yin, V. Spagnolo, S. Jia, F.K. Tittel, Single-tube on-beam quartz-enhanced photoacoustic spectroscopy, Opt. Lett. 41 (2016) 978–981.
[67] H. Zheng, L. Dong, A. Sampaolo, P. Patimisco, W. Ma, L. Zhang, W. Yin, L. Xiao, V. Spagnolo, S. Jia, F.K. Tittel, Overtone resonance enhanced single-tube on-beam quartz enhanced photoacoustic spectrophone, Appl. Phys. Lett. 109 (2016), 111103.
[68] P. Patimisco, A. Sampaolo, H. Zheng, L. Dong, F.K. Tittel, V. Spagnolo, Quartz–enhanced photoacoustic spectrophones exploiting custom tuning forks: a review, Adv. Phys. 2 (2017) 169–187.
[69] M. Giglio, A. Sampaolo, P. Patimisco, H. Zheng, H. Wu, L. Dong, F.K. Tittel, V. Spagnolo, Single-tube on beam quartz-enhanced photoacoustic spectrophones exploiting a custom quartz tuning fork operating in the overtone mode, Quant. Sens. Nano Electron. Photonics XIV 10111 (2017), 1011107.
[70] L. Dong, H. Wu, H. Zheng, Y. Liu, X. Liu, W. Jiang, L. Zhang, W. Ma, W. Ren, W. Yin, S. Jia, F.K. Tittel, Double acoustic microresonator quartz-enhanced photoacoustic spectroscopy, Opt. Lett. 39 (2014) 2479–2482.
[71] Y. Liu, J. Chang, J. Lian, Z. Liu, Q. Wang, Z. Qin, Quartz-enhanced photoacoustic spectroscopy with right-angle prism, Sensors 16 (2016) 214.
[72] R. Cui, H. Wu, L. Dong, W. Chen, F.K. Tittel, Multiple-sound-source-excitation quartz-enhanced photoacoustic spectroscopy based on a single-line spot pattern multi-pass cell, Appl. Phys. Lett. 118 (2021), 161101.
[73] G. Aoust, R. Levy, M. Raybaut, A. Godard, J.M. Melkonian, M. Lefebvre, Theoretical analysis of a resonant quartz-enhanced photoacoustic spectroscopy sensor, Appl. Phys. B 123 (2017) 63.
[74] K. Liu, X. Guo, H. Yi, W. Chen, W. Zhang, X. Gao, Off-beam quartz-enhanced photoacoustic spectroscopy, Opt. Lett. 34 (2009) 1594–1596.
[75] H. Yi, K. Liu, S. Sun, W. Zhang, X. Gao, Theoretical analysis of off beam quartz-enhanced photoacoustic spectroscopy sensor, Opt. Commun. 285 (2012) 5306–5312.
[76] R. Rousseau, Z. Loghmari, M. Bahriz, K. Chamassi, R. Teissier, A.N. Baranov, A. Vicet, Off-beam QEPAS sensor using an 11-μm DFB-QCL with an optimized acoustic resonator, Opt. Express 27 (2019) 7435–7446.
[77] T. Rück, R. Bierl, F.M. Matysik, NO2 trace gas monitoring in air using off-beam quartz enhanced photoacoustic spectroscopy (QEPAS) and interference studies towards CO_2, H2O and acoustic noise, Sens. Actuators B-Chem. 255 (2017) 2462–2471.
[78] L. Hu, C. Zheng, J. Zheng, Y. Wang, F.K. Tittel, Quartz tuning fork embedded off-beam quartz-enhanced photoacoustic spectroscopy, Opt. Lett. 44 (2019) 2562–2565.
[79] Z. Liang, S. Qiao, Y. Ma, Acoustic microresonator based in-plane quartz-enhanced photoacoustic spectroscopy sensor with a line interaction mode, Opt. Lett. 47 (2022) 1295–1298.
[80] H. Yi, W. Chen, S. Sun, K. Liu, T. Tan, X. Gao, T-shape microresonator-based high sensitivity quartz-enhanced photoacoustic spectroscopy sensor, Opt. Express 20 (2012) 9187–9196.
[81] H. Yi, W. Chen, A. Vicet, Z. Cao, X. Gao, T. Nguyen-ba, M. Jahjah, Y. Rouillard, L. Nähle, M. Fischer, T-shape microresonator-based quartz-enhanced photoacoustic spectroscopy for ambient methane monitoring using 3.38-μm antimonide-distributed feedback laser diode, Appl. Phys. B 116 (2014) 423–428.
[82] Y. Ma, Y. Hong, S. Qiao, Z. Lang, X. Liu, H-shaped acoustic micro-resonator-based quartz-enhanced photoacoustic spectroscopy, Opt. Lett. 47 (2022) 601–604.

[83] H. Lv, H. Zheng, Y. Liu, Z. Yang, Q. Wu, H. Lin, B.A.Z. Montano, W. Zhu, J. Yu, R. Kan, Z. Chen, F.K. Tittel, Radial-cavity quartz-enhanced photoacoustic spectroscopy, Opt. Lett. 46 (2021) 3917–3920.
[84] S. Borri, P. Patimisco, A. Sampaolo, H.E. Beere, D.A. Ritchie, M.S. Vitiello, G. Scamarcio, V. Spagnolo, Terahertz quartz enhanced photo-acoustic sensor, Appl. Phys. Lett. 103 (2013), 021105.
[85] P. Patimisco, S. Borri, A. Sampaolo, H.E. Beere, D.A. Ritchie, M.S. Vitiello, Gaetano Scamarcio, V. Spagnolo, A quartz enhanced photo-acoustic gas sensor based on a custom tuning fork and a terahertz quantum cascade laser, Analyst 139 (2014) 2079–2087.
[86] P. Patimisco, A. Sampaolo, L. Dong, M. Giglio, G. Scamarcio, F.K. Tittel, V. Spagnolo, Analysis of the electro-elastic properties of custom quartz tuning forks for optoacoustic gas sensing, Sens. Actuators B-Chem. 227 (2016) 539–546.
[87] M. Giglio, A. Elefante, P. Patimisco, A. Sampaolo, F. Sgobba, H. Rossmadl, V. Mackowiak, H. Wu, F.K. Tittel, L. Dong, V. Spagnolo, Quartz-enhanced photoacoustic sensor for ethylene detection implementing optimized custom tuning fork-based spectrophone, Opt. Express 27 (2019) 4271–4280.
[88] B. Sun, A. Zifarelli, H. Wu, S.D. Russo, S. Li, P. Patimisco, L. Dong, V. Spagnolo, Mid-infrared quartz-enhanced photoacoustic sensor for ppb-level CO detection in a SF6 gas matrix exploiting a T-grooved quartz tuning fork, Anal. Chem. 92 (2020) 13922–13929.
[89] J. Hayden, M. Giglio, A. Sampaolo, V. Spagnolo, B. Lendl, Mid-infrared intracavity quartz-enhanced photoacoustic spectroscopy with pptv – Level sensitivity using a T-shaped custom tuning fork, Photoacoustics 25 (2022), 100330.
[90] Y. Ma, Y. He, Y. Tong, X. Yu, F.K. Tittel, Quartz-tuning-fork enhanced photothermal spectroscopy for ultra-high sensitive trace gas detection, Opt. Express 26 (24) (2018) 32103–32110.
[91] Y. Ma, W. Feng, S. Qiao, Z. Zhao, S. Gao, Y. Wang, Hollow-core anti-resonant fiber based light-induced thermoelastic spectroscopy for gas sensing, Opt. Express 30 (17) (2022) 18836–18844.
[92] Huadan Zheng, Yihua Liu, Haoyang Lin, Bin Liu, Xiaohang Gu, Dongquan Li, Bincheng Huang, Yichao Wu, Linpeng Dong, Wenguo Zhu, Jieyuan Tang, Heyuan Guan, Huihui Lu, Yongchun Zhong, Junbin Fang, Yunhan Luo, Jun Zhang, Jianhui Yu, Zhe Chen, Frank K. Quartz-enhanced photoacoustic spectroscopy employing pilot line manufactured custom tuning forks, ISSN 2213-5979, Photoacoustics 17 (2020), 100158, https://doi.org/10.1016/j.pacs.2019.100158.
[93] J. Uotila, Use of the Optical Cantilever Microphone in Photoacoustic Spectroscopy, TURUN YLIOPISTO, Turku, Finland, 2009.
[94] S. Sinisalo, H. Karlsson, OPO-based photoacoustic spectroscopy speeds up gas analysis, Photonics Spectra 48 (2014) 30–34.
[95] A. Garca-Valenzuela, J. Villatoro, Noise in optical measurements of cantilever deflections, J. Appl. Phys. 84 (1998) 58–63.
[96] R.A. Coutu, I.R. Medvedev, D.T. Petkie, Improved sensitivity MEMS cantilever sensor for terahertz photoacoustic spectroscopy, Sensors 6 (2016) 251.
[97] N.E. Glauvitz, R.A. Coutu, I.R. Medvedev, D.T. Petkie, Terahertz photoacoustic spectroscopy using a MEMS cantilever sensor, J. Micro Syst. 24 (2015) 216–223.
[98] T. Laurila, H. Cattaneo, V. Koskinen, J. Kauppinen, R. Hernberg, Diode laser-based photoacoustic spectroscopy with interferometrically-enhanced cantilever detection, Opt. Express 13 (2005) 2453–2458.
[99] C.B. Hirschmann, J. Lehtinen, J. Uotila, S. Ojala, R.L. Keiski, Sub-ppb detection of formaldehyde with cantilever enhanced photoacoustic spectroscopy using quantum cascade laser source, Appl. Phys. B 111 (2013) 603–610.
[100] T. Mikkonen, C. Amiot, A. Aalto, K. Patokoski, G. Genty, J. Toivonen, Broadband cantilever-enhanced photoacoustic spectroscopy in the mid-IR using supercontinuum, Opt. Lett. 43 (2018) 5094–5097.
[101] T. Tomberg, M. Vainio, T. Hieta, L. Halonen, Sub-parts-per-trillion level sensitivity in trace gas detection by cantilever-enhanced photo-acoustic spectroscopy, Sci. Rep. 8 (2018) 1848.
[102] M. Fatima, T. Hausmaninger, T. Tomberg, J. Karhu, M. Vainio, T. Hieta, G. Genoud, Radiocarbon dioxide detection using cantilever-enhanced photoacoustic spectroscopy, Opt. Lett. 46 (2021) 2083–2086.
[103] J. Peltola, T. Hieta, M. Vainio, Parts-per-trillion-level detection of nitrogen dioxide by cantilever-enhanced photo-acoustic spectroscopy, Opt. Lett. 40 (13) (2015) 2933–2936.
[104] J. Peltola, M. Vainio, T. Hieta, et al., High sensitivity trace gas detection by cantilever-enhanced photoacoustic spectroscopy using a mid-infrared continuous-wave optical parametric oscillator, Opt. Express 21 (8) (2013) 10240–10250.
[105] H. Cheng, J. Tang, X. Zhang, Y. Li, J. Hu, Y. Zhang, S. Mao, S. Xiao, Simultaneous detection of C_2H_2 and CO based on cantilever-enhanced photoacoustic spectroscopy, IEEE Trans. Instrum. Meas. 70 (2021) 1–10.
[106] Wei Wei, Yong Zhu, Cheng Lin, Li Tian, Zhuwen Xu, Jinpeng Nong, All-optical cantilever-enhanced photoacoustic spectroscopy in the open environment, Int. J. Thermophys. 36 (2015) 1116–1122.
[107] Y. Cao, W. Jin, H.L. Ho, J. Ma, Miniature fiber-tip photoacoustic spectrometer for trace gas detection, Opt. Lett. 38 (2013) 434–436.
[108] Z. Gong, K. Chen, Y. Yang, X. Zhou, W. Peng, Q. Yu, High-sensitivity fiber-optic acoustic sensor for photoacoustic spectroscopy based traces gas detection, Sens. Actuators B-Chem. 247 (2017) 290–295.
[109] Min Guo, Ke Chen, Chenxi Li, Lin Xu, Guangyin Zhang, Nan Wang, Chenyang Li, Fengxiang Ma, Zhenfeng Gong, Qingxu Yu, High-Sensitivity Silicon Cantilever-Enhanced Photoacoustic Spectroscopy Analyzer with Low Gas Consumption, Anal. Chem. 94 (2022) 1151–1157.
[110] Ke Chen, Qingxu Yu, Zhenfeng Gong, Min Guo, Chao Qu, Ultra-high sensitive fiber-optic Fabry-Perot cantilever enhanced resonant photoacoustic spectroscopy, Sens. Actuators B 268 (2018) 205–209.
[111] Ke Chen, Hong Deng, Min Guo, Chen Luo, Shuai Liu, Bo Zhang, Fengxiang Ma, Feng Zhu, Zhenfeng Gong, Wei Peng, Qingxu Yu, Tube-cantilever double resonance enhanced fiber-optic photoacoustic spectrometer, Opt. Laser Technol. 123 (2020), 105894.
[112] Chenyang Li, Min Guo, Bo Zhang, Chenxi Li, Beilei Yang, Ke Chen, Miniature single-fiber photoacoustic sensor for methane gas leakage detection, Opt. Lasers Eng. 149 (2022), 106792.
[113] Sheng Zhou, Martin Slaman, Davide Iannuzzi, Demonstration of a highly sensitive photoacoustic spectrometer based on a miniaturized all-optical detecting sensor, Opt. Express 25 (2017) 17541–17548.
[114] J. Lu, T. Ikehara, Y. Zhang, T. Mihara, R. Maeda, Mechanical quality factor of microcantilevers for mass sensing applications, Int. Soc. Opt. Photonics (2007) 68001.
[115] Z. Sheng, D. Iannuzzi, A fiber-tip photoacoustic sensor for in situ trace gas detection, Rev. Sci. Instrum. 90 (2) (2019), 023102.
[116] Sheng Zhou, Davide, et al., Immersion photoacoustic spectrometer (iPAS) for arcing fault detection in power transformers, Opt. Lett. 44 (15) (2019) 3741–3744.

Fupeng Wang received the Ph.D degree in Optical Engineering from Shandong University (Jinan) and University of Washington (Seattle), in 2019. He is currently an Assistant Professor at Ocean University of China (Tsingtao). His research interest includes tunable laser absorption spectroscopy (TDLAS), photoacoustic spectroscopy (PAS), non-dispersive infrared spectroscopy (NDIR), and spectroscopy-based engineering applications in ocean detection and atmosphere analysis.

Yaopeng Cheng was born in Suzhou, China in 2000. He is currently working towards his B.E. degree at College of Information Science and Engineering, Ocean University of China (OUC), Qingdao, China. His research interests include tunable diode laser absorption spectroscopy, photoacoustic spectroscopy and Fourier-domain optical coherent absorption spectroscopy.

Qingsheng Xue received the Ph. D degree in Optical Engineering from Changchun Institute of Optics. Fine Mechanics and Physics, Chinese Academy of Sciences in 2010. He is currently a professor at Ocean University of China (Tsingtao). His research interests include optical design, hyperspectral imaging, development and applications of optical instruments for ocean detection.

Qiang Wang is currently a full professor at the State Key Laboratory of Applied Optics of Changchun Institute of Optics, Fine Mechanics and Physics, Chinese Academy of Sciences. He received his B.S. degree in Electronic Science and Technology in 2011 and Ph.D. degree in Optical Engineering in 2016 from Shandong University. After his graduate study, he worked as a postdoctoral fellow at the Chinese University of Hong Kong and Max Planck Institute of Quantum Optics successively. His recent research interest includes laser spectroscopy, optical sensing, and engineering application of trace gas analysis in atmosphere, deep sea, and public health.

Rui Liang was born in Shanxi Province, China, in October 1995. He received the B.S. in optoelectronic information science and engineering from the Nanyang Institute of Technology, Henan, China. He is currently pursuing the master degree at the College of Physics and Optoelectronic Engineering, Ocean University of China, Qingdao, China. His current research interest includes optical sensing device and engineering application.

Jinghua Wu was born in Dezhou, Shandong, China in 1999. In 2021, he graduated from Nanyang Institute of Technology and obtained a bachelor's degree in Optoelectronic Information Science and engineering. He is engaged in the non-dispersive infrared CO_2 sensor development and application for ocean detection.

Jiachen Sun was born in Shanxi Province, China, in December 1995. He received the B.S. degree from Shandong University in 2018. He is currently pursuing the Ph. D degree in the Department of Optical Engineering at the Institution of Information Science and Engineering, Shandong University, China. He is currently major in tunable diode laser absorption spectroscopy and deep learning.

Cunguang Zhu was born in Liaocheng, Shandong, China, in 1985. He received the Ph.D. degree in optoelectronic engineering from Shandong University, Jinan, China, in 2015. He is currently with the School of Physics Science and Information Technology, Liaocheng University, Liaocheng. His current research interests include optical gas sensing devices, optical fiber sensor fabrication, and engineering applications.

Qian Li was born in Weihai, China in 1993. He received the B.S. in electrical engineering and automation engineering from the Harbin Institute of Technology (HIT), Harbin, China, in 2015. From 2015–2020, he majored in circuits and systems at Changchun Institute of Optics, Fine Mechanics and Physics, Chinese Academy of Sciences, China with a Ph.D. degree. He is currently a lecturer in the College of Information Science and Engineering, Ocean University of China. He mainly engaged in weak signal detection.